



**HAL**  
open science

# Variable Iron Mineralogy and Redox Conditions Recorded in Ancient Rocks Measured by In Situ Visible/Near-Infrared Spectroscopy at Jezero Crater, Mars

L Mandon, B L Ehlmann, R C Wiens, B J Garczynski, B H N Horgan, T Fouchet, M Loche, E Dehouck, P Gasda, J R Johnson, et al.

► **To cite this version:**

L Mandon, B L Ehlmann, R C Wiens, B J Garczynski, B H N Horgan, et al.. Variable Iron Mineralogy and Redox Conditions Recorded in Ancient Rocks Measured by In Situ Visible/Near-Infrared Spectroscopy at Jezero Crater, Mars. *Journal of Geophysical Research. Planets*, 2024, 129 (7), pp.e2023JE008254. 10.1029/2023je008254 . hal-04658026

**HAL Id: hal-04658026**

**<https://hal.science/hal-04658026>**

Submitted on 22 Jul 2024








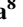


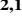


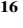




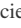
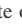
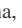
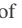
**HAL** is a multi-disciplinary open access archive for the deposit and dissemination of scientific research documents, whether they are published or not. The documents may come from teaching and research institutions in France or abroad, or from public or private research centers.

L'archive ouverte pluridisciplinaire **HAL**, est destinée au dépôt et à la diffusion de documents scientifiques de niveau recherche, publiés ou non, émanant des établissements d'enseignement et de recherche français ou étrangers, des laboratoires publics ou privés.

### Special Collection:

The Perseverance Rover's  
Exploration of the Western Fan  
Front, Jezero Crater, Mars

# Variable Iron Mineralogy and Redox Conditions Recorded in Ancient Rocks Measured by In Situ Visible/Near-Infrared Spectroscopy at Jezero Crater, Mars

L. Mandon<sup>1,2</sup> , B. L. Ehlmann<sup>1</sup> , R. C. Wiens<sup>3</sup> , B. J. Garczynski<sup>4</sup> , B. H. N. Horgan<sup>3</sup> , T. Fouchet<sup>5</sup> , M. Loche<sup>6</sup> , E. Dehouck<sup>7</sup> , P. Gasda<sup>8</sup> , J. R. Johnson<sup>9</sup> , A. Broz<sup>3</sup> , J. I. Núñez<sup>9</sup> , M. S. Rice<sup>4</sup> , A. Vaughan<sup>10</sup> , C. Royer<sup>3</sup> , F. Gómez<sup>11</sup> , A. M. Annex<sup>12,13</sup> , O. Beyssac<sup>14</sup> , O. Forni<sup>6</sup> , A. Brown<sup>15</sup> , J. F. Bell III<sup>16</sup> , and S. Maurice<sup>6</sup> 

### Key Points:

- In situ reflectance data measured with Mars 2020 show variable Fe mineralogy in sedimentary rocks at Jezero crater
- Strata exposed at the fan front experienced stronger oxidative water-rock interactions compared to the upper fan and igneous crater floor
- We identify cm-scale color banding correlated with Fe-oxide variability that likely indicates time variation in redox

### Supporting Information:

Supporting Information may be found in the online version of this article.

### Correspondence to:

L. Mandon,  
lmandon@caltech.edu

### Citation:

Mandon, L., Ehlmann, B. L., Wiens, R. C., Garczynski, B. J., Horgan, B. H. N., Fouchet, T., et al. (2024). Variable iron mineralogy and redox conditions recorded in ancient rocks measured by in situ visible/near-infrared spectroscopy at Jezero crater, Mars. *Journal of Geophysical Research: Planets*, 129, e2023JE008254. <https://doi.org/10.1029/2023JE008254>

Received 15 DEC 2023

Accepted 15 APR 2024

### Author Contributions:

**Conceptualization:** L. Mandon

**Formal analysis:** L. Mandon

**Funding acquisition:** B. L. Ehlmann, R. C. Wiens, J. F. Bell III, S. Maurice

**Investigation:** L. Mandon, B. J. Garczynski, B. H. N. Horgan, E. Dehouck, J. R. Johnson, A. Broz,

© 2024 The Author(s).

This is an open access article under the terms of the [Creative Commons Attribution-NonCommercial](https://creativecommons.org/licenses/by-nc/4.0/) License, which permits use, distribution and reproduction in any medium, provided the original work is properly cited and is not used for commercial purposes.

<sup>1</sup>Division of Geological and Planetary Sciences, California Institute of Technology, Pasadena, CA, USA, <sup>2</sup>University of Grenoble Alpes, CNRS, IPAG, Grenoble, France, <sup>3</sup>Earth, Atmospheric, and Planetary Sciences, Purdue University, West Lafayette, IN, USA, <sup>4</sup>Western Washington University Department of Geology, Bellingham, WA, USA, <sup>5</sup>LESIA, Observatoire de Paris, Université PSL, CNRS, Sorbonne Université, Université Paris-Cité, Meudon, France, <sup>6</sup>Institut de Recherche en Astrophysique et Planétologie, Université de Toulouse 3 Paul Sabatier, CNRS, CNES, France, <sup>7</sup>Université Claude Bernard Lyon1, LGL-TPE, UMR 5276, CNRS, ENSL, UJM, Villeurbanne, France, <sup>8</sup>Los Alamos National Laboratory, Los Alamos, NM, USA, <sup>9</sup>Johns Hopkins University Applied Physics Laboratory, Laurel, MD, USA, <sup>10</sup>Apogee Engineering, LLC, Flagstaff, AZ, USA, <sup>11</sup>Centro de Astrobiología (INTA-CSIC), Madrid, Spain, <sup>12</sup>SETI Institute Carl Sagan Center for Research, Mountain View, CA, USA, <sup>13</sup>NASA Ames Research Center, Moffett Field, CA, USA, <sup>14</sup>Institut de Minéralogie, de Physique des Matériaux et de Cosmochimie, CNRS UMR 7590, Sorbonne Université, Muséum National d'Histoire Naturelle, Paris, France, <sup>15</sup>Plancius Research, Severna Park, MD, USA, <sup>16</sup>School of Earth and Space Exploration, Arizona State University, Tempe, AZ, USA

**Abstract** Using relative reflectance measurements from the Mastcam-Z and SuperCam instruments on the Mars 2020 *Perseverance* rover, we assess the variability of Fe mineralogy in Noachian/Hesperian-aged rocks at Jezero crater. The results reveal diverse Fe<sup>3+</sup> and Fe<sup>2+</sup> minerals. The igneous crater floor, where small amounts of Fe<sup>3+</sup>-phyllosilicates and poorly crystalline Fe<sup>3+</sup>-oxyhydroxides have been reported, is spectrally similar to most oxidized basalts observed at Gusev crater. At the base of the western Jezero sedimentary fan, new spectral type points to an Fe-bearing mineral assemblage likely dominated by Fe<sup>2+</sup>. By contrast, most strata exposed at the fan front show signatures of Fe<sup>3+</sup>-oxides (mostly fine-grained crystalline hematite), Fe<sup>3+</sup>-sulfates (potentially copiapites), strong signatures of hydration, and among the strongest signatures of red hematite observed in situ, consistent with materials having experienced vigorous water-rock interactions and/or higher degrees of diagenesis under oxidizing conditions. The fan top strata show hydration but little to no signs of Fe oxidation likely implying that some periods of fan construction occurred either during a reduced atmosphere era or during short-lived aqueous activity of liquid water in contact with an oxidized atmosphere. We also report the discovery of alternating cm-scale bands of red and gray layers correlated with hydration and oxide variability, which has not yet been observed elsewhere on Mars. This could result from syn-depositional fluid chemistry variations, possibly as seasonal processes, or diagenetic overprint of oxidized fluids percolating through strata having variable permeability.

**Plain Language Summary** The oxidation states of the atmosphere and waters (whether rich or poor in oxidants such as oxygen) of Mars and their evolution are poorly constrained but can be recorded in the iron (Fe) mineralogy of rocks. Using data from the *Perseverance* rover, we analyzed the Fe mineralogy of ~4–3 Ga old rocks from an ancient lake at Jezero crater. Oxidized Fe is found in igneous rocks and lowermost portions of sedimentary rocks, carried by clays and poorly crystalline oxides in the former and by sulfates and crystalline oxides in the latter, pointing to past action of oxidizing fluids, affecting more intensely the sedimentary rocks. Fe shows poor to no signs of oxidation in the uppermost strata, which might be evidence for a reducing atmosphere during sediment deposition or that the aqueous environment was too cold or too short-lived to oxidize minerals. We also report Fe mineralogy variability at the cm-scale in alternating colored layers, which has not been observed previously on Mars and could possibly mean that seasonal processes are recorded at Jezero crater.

J. I. Núñez, M. S. Rice, A. Vaughan,  
O. Forni

**Methodology:** L. Mandon, C. Royer,  
A. M. Annex, O. Forni

**Project administration:** B. L. Ehlmann,  
R. C. Wiens, J. F. Bell III, S. Maurice

**Supervision:** B. L. Ehlmann, R. C. Wiens,  
B. H. N. Horgan

**Writing – original draft:** L. Mandon,  
F. Gómez

**Writing – review & editing:** L. Mandon,  
B. L. Ehlmann, R. C. Wiens,

B. J. Garczynski, B. H. N. Horgan,

T. Fouchet, M. Loche, E. Dehouck,

P. Gasda, J. R. Johnson, A. Broz,

O. Beyssac, A. Brown

## 1. Introduction

### 1.1. Importance of Fe-Mineralogy on Mars and Past Redox Conditions

Iron (Fe) is one of the major components of the Martian crust (averaging 11–19 wt.%, e.g., Boynton et al., 2007) and is found in a variety of primary and secondary minerals. It has a solubility sensitive to oxidation–reduction conditions (redox), where  $\text{Fe}^{3+}$  is substantially less soluble than  $\text{Fe}^{2+}$  and only dissolves in acidic fluids (Hem & Cropper, 1962). Hence, the Martian Fe mineralogic record can be used to probe past processes related to atmospheric composition and alteration of rocks by surface and ground waters. Furthermore, the evolution of these conditions through time is closely related to the investigation of past climate. Understanding the state and evolution of redox conditions is also important to assess the habitability and fate of potential organic matter and biosignatures. Indeed, organic matter is unstable under oxidizing conditions, and reducing conditions are conventionally thought to be more favorable to pre-biotic chemistry (e.g., Miller, 1953). Furthermore, reducing atmospheric species ( $\text{H}_2$ ,  $\text{CH}_4$ ) have been proposed to play a major role in warming early Mars (Ramirez et al., 2014; Wordsworth et al., 2017). On the other hand, specific  $\text{Fe}^{3+}$ -oxides (e.g., crystalline hematite) can permineralize biogenic structures (Allen et al., 2001), and oxidizing atmospheric conditions can drive redox disequilibria, which can generate useful energy for biological activity (e.g., Russell & Hall, 1997). It is thus important to recognize redox conditions recorded in rocks at Jezero crater (the Mars 2020 rover landing site) that interacted with liquid water during the Noachian (>3.7 Ga) and Hesperian (3.7–3.0 Ga) eras and which are being selected for collection and return to Earth (Bosak et al., 2024; Farley et al., 2020; Simon et al., 2023).

Our initial understanding of the Fe-mineralogy of the surface of Mars comes from its distinctive red-orange color, caused by poorly crystalline, nanophase  $\text{Fe}^{3+}$ -oxides in the ubiquitous Martian dust (Morris et al., 2000). Early landed investigation started in the 1970s with Viking missions, which revealed the enrichment in Fe of the Martian soil compared to terrestrial soils (Clark et al., 1976). They also showed the highly oxidizing nature of the Martian surface, possibly from UV radiation and/or oxidizing chemical components (Biemann et al., 1977), such as the perchlorates later detected at the Phoenix and Mars Science Laboratory (MSL) landing sites (Glavin et al., 2013; Hecht et al., 2009; Navarro-González et al., 2010). Using orbital data from the Thermal Emission Spectrometer (TES), Christensen, Bandfield, Smith, et al. (2000) showed the predominance of basalts underneath the thin and global dust layer. At the same time, Christensen, Bandfield, Clark, et al. (2000) detected widespread coarse-grained crystalline black/gray hematite in the Hesperian-aged region of Meridiani Planum, which contrasted with the fine-grained poorly crystalline red hematite present in the dust, suggesting variable formation processes of Fe-oxides.

Analysis of the visible and near-infrared (VISIR) reflectance spectra in the 0.35–5.1  $\mu\text{m}$  range collected by the Observatoire pour la Minéralogie, l’Eau, les Glaces et l’Activité (OMEGA) marked a shift in our vision of the Martian mineralogy, which revealed abundant hydrated minerals on ancient terrains, including Fe/Mg- and Al-rich phyllosilicates primarily on Noachian surfaces, and sulfates primarily on Hesperian surfaces (Bibring et al., 2005; Gendrin et al., 2005; Poulet et al., 2005). Both  $\text{Fe}^{2+}$  and  $\text{Fe}^{3+}$ -bearing phyllosilicate species were reported (Michalski et al., 2010). At a global scale, the sulfate-bearing deposits typically occur in close association with Fe-oxides such as crystalline hematite (Bibring et al., 2007). OMEGA also revealed the distribution of mafic igneous minerals on the surface, with both olivine and low-Ca pyroxene being widely observed over crustal and igneous provinces, and low-Ca pyroxene being broadly restricted to the most ancient early Noachian terrains (Mustard et al., 2005). Using a similar technique of VISIR reflectance spectroscopy as OMEGA at a finer spatial scale and in the 0.36–3.9  $\mu\text{m}$  spectral range, the Compact Reconnaissance Imaging Spectrometer for Mars (CRISM) revealed the diversity of alteration phases, several of which incorporate Fe in their structure, including high temperature minerals (e.g., serpentine, chlorite, micas) or Fe/Mg-carbonates (Carter et al., 2013; Ehlmann et al., 2009, 2011; Mustard et al., 2008).

Confirming the orbital detection of crystalline gray hematite at Meridiani Planum, the Mars Exploration Rovers (MERs) also revealed the presence of  $\text{Fe}^{3+}$ -sulfates (including jarosite) that formed in acidic waters, both in soils at the Gusev site and within bedrock at Meridiani Planum (Morris et al., 2006b, 2008). In Gale crater sedimentary rocks, X-ray diffraction measurement by the Chemistry and Mineralogy (CheMin) instrument coupled with elemental analysis by the Alpha Particle X-ray Spectrometer (APXS) showed that  $\text{Fe}^{2+}$  and  $\text{Fe}^{3+}$ -phyllosilicates, magnetite, hematite, and Fe-bearing amorphous materials were the principal carriers of Fe, with occasional minor jarosite, siderite, and other phases (Bristow et al., 2018; Rampe et al., 2017; Rampe, Blake, et al., 2020; Smith et al., 2021; Vaniman et al., 2014). Clay minerals detected by CheMin included trioctahedral smectites at the base

of the sediment stratigraphy, with a transition to dioctahedral smectites going upwards (Bristow et al., 2015, 2018). Co-existence of hematite- and magnetite-bearing deposits was suggested over a short interval low in the stratigraphy (Hurowitz et al., 2017). Higher in the stratigraphy, Fe<sup>3+</sup>-phyllosilicates and hematite became more prevalent (Bristow et al., 2018), and focused Fe deposition by Fe-bearing diagenetic fluids played a key role in the creation of the Vera Rubin ridge (Fraeman, Edgar, et al., 2020). Of interest for the oxidation history of the altering fluids on Mars, the presence of Mn-oxides in the bedrock of the Hesperian Gale crater (Lanza et al., 2014) and as coatings on rocks at the Noachian-aged Endeavor Crater (Arvidson et al., 2016) both required liquid water and more oxidizing conditions than Fe<sup>3+</sup>-oxides.

Very early in the history of Mars (>4.4 Ga), loss of H<sub>2</sub> into space drove an excess of O in the atmosphere (e.g., McElroy, 1972). This atmosphere and consequently the rock-altering fluids in contact with it hence likely became quickly oxidizing. Meteorite studies have shown that the Martian mantle is broadly more reduced than the terrestrial mantle (e.g., Wadhwa, 2001); hence, any volcanic activity would supply reduced species to the atmosphere. In this context, climate modeling suggests that the Noachian atmosphere could have been at least episodically reducing as a result of significant volcanic outgassing of reduced species compensating loss of H<sub>2</sub> into space (e.g., Ramirez et al., 2014).

In a scenario where the surface environment is oxidizing, such as what is most common on Earth, expected products of water-rock interactions include ferric species such as Fe<sup>3+</sup>-phyllosilicates, Fe<sup>3+</sup>-oxides and salts. Using thermodynamic calculations, Chevrier et al. (2007) investigated the chemical conditions required to form the widespread clay-bearing deposits observed from orbit over Noachian terrains and proposed that dioctahedral Fe<sup>3+</sup>-smectites formed by direct precipitation from chemical weathering of the mafic crust under the action of oxidizing fluids support a broadly oxidizing surface during the Noachian.

Later laboratory alteration experiments performed by Chemtob et al. (2015, 2017) showed that dioctahedral Fe<sup>3+</sup>-smectites can form from oxidation of Fe<sup>2+</sup>-smectite precursors, arguing that the presence of Fe<sup>3+</sup>-smectites on Noachian terrains does not necessarily relate to an oxidizing surface at the time of formation of widespread clay mineral provinces but instead a later overprinting process. Supporting this hypothesis, Dehouck et al. (2014, 2016) conducted alteration experiments of mafic minerals under a dense CO<sub>2</sub> atmosphere and reported inhibition of Fe/Mg-phyllosilicate formation under highly oxidizing conditions, suggesting that their formation on Mars occurred under poorly oxidizing to reduced conditions.

In a scenario where the atmosphere is oxidizing but alteration occurs in groundwaters, oxidation of Fe in secondary minerals is limited. For example, alteration may produce Fe<sup>2+</sup>/Mg-smectites (or serpentine and chlorite at higher temperature) as groundwater fluids in basalts are buffered to a reduced state, a result of reaction with Fe<sup>2+</sup> in the rocks along the flow path. Surveying the distribution and diversity of clay minerals using OMEGA and CRISM, Ehlmann et al. (2011) reported the dominance of Fe/Mg-smectites in association with chlorite, compared to Al/Fe<sup>3+</sup>-smectites and salts assemblages that were interpreted to have formed in weathering environments in contact with the atmosphere (e.g., Bishop et al., 2008). As a consequence, they proposed that the most sustained aqueous environment on Mars would have been in Noachian groundwater.

An alternative model is the case where the surface is broadly reducing, and that could be compared to the increased H<sub>2</sub> epochs predicted by some atmospheric models (e.g., Ramirez et al., 2014). Based on mineralogy, distinguishing this environment from a low temperature reducing groundwater environment is difficult, because, except for salts such as carbonates, broadly similar species are expected to form in both cases.

More complicated systems exist and have been suggested for Mars: at Gale crater, Hurowitz et al. (2017) interpreted the hematite and magnetite in the sediments comprising the Murray Formation as authigenic deposition at various depths in a shallow redox stratified lake in contact with an oxidizing surface (from UV radiations or oxygenated atmosphere).

Finally, diagenetic processes complicate the interpretation of potential scenarios, as they can alter the initial Fe mineralogy. In particular, at the Hesperian sites of Meridiani Planum and Gale crater, crystalline hematite has been attributed by several authors to episode(s) of oxidizing fluid circulation subsequent to initial deposition (e.g., Horgan, Johnson, et al., 2020; McLennan et al., 2005; Rampe et al., 2017).

## 1.2. The Mars 2020 Mission

In February 2021, the Mars 2020 mission *Perseverance* rover landed in Jezero crater. This crater, which formed ~3.8–4 Ga ago (Mandon et al., 2020), hosted a lake and preserved fluvial-deltaic sediments (Fassett & Head, 2005; Goudge et al., 2017; Mangold et al., 2021). Fe/Mg smectites and carbonates were identified from orbit as well as units with low-Ca pyroxene and olivine (Ehlmann et al., 2008, 2009; Horgan, Anderson, et al., 2020). Sedimentary rocks explored by the rover in the western fan (Ives et al., 2023; Stack et al., 2024) most likely correspond to a period of deposition in the Hesperian (Mangold et al., 2020). The main geological goals of the mission are to investigate past climate and habitability and seek biosignatures by in situ analysis of the terrains and collection of samples to be returned to Earth (Farley et al., 2020).

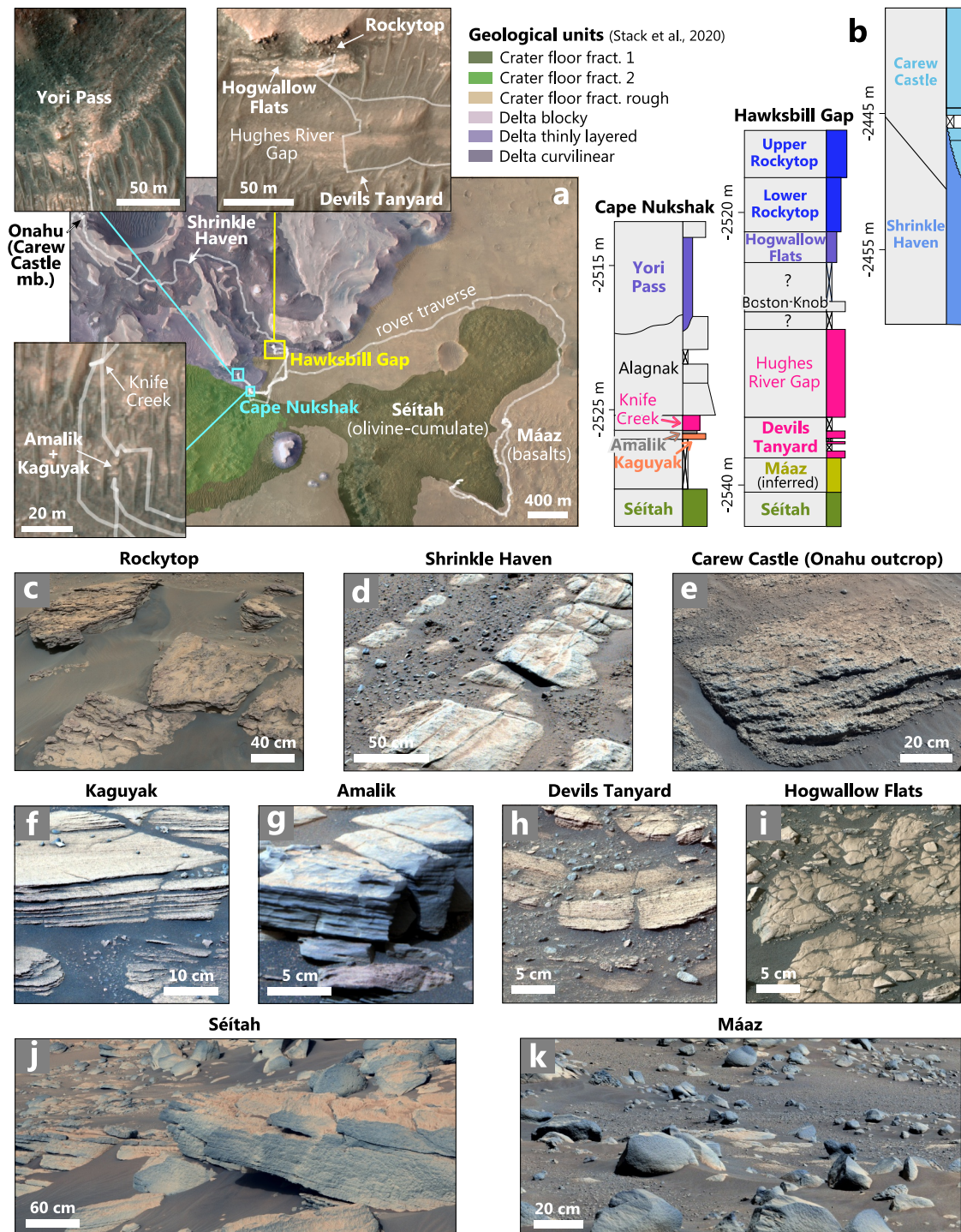
Here, we investigate the reflectance of rocks by combining visible and near-infrared (VISIR) measurements from the Mastcam-Z and SuperCam instruments onboard *Perseverance* to assess the variability of Fe-bearing phases within and between members of the sedimentary stratigraphy of the delta fan, and whether the Fe-bearing materials represent reduced or oxidized minerals. Specifically, we combine SuperCam VISIR spectra and Mastcam-Z multispectral observations, mostly on the same rock targets. We compare their spectral signatures to those of igneous rocks present on the crater floor (below the sedimentary units) as well as similar data from prior Mars landing sites to understand the changes in weathering and redox state. This work is conducted in parallel with others that define the fan stratigraphy (Stack et al., 2024), present the overviews of SuperCam (Dehouck et al., 2023) and Mastcam-Z (Núñez et al., 2023) results from Jezero's western fan, or use other rover instruments to interrogate composition (e.g., Hurowitz et al., 2023; Phua et al., 2024).

## 2. Previous In Situ Studies at Jezero: Crater Floor Igneous Rocks

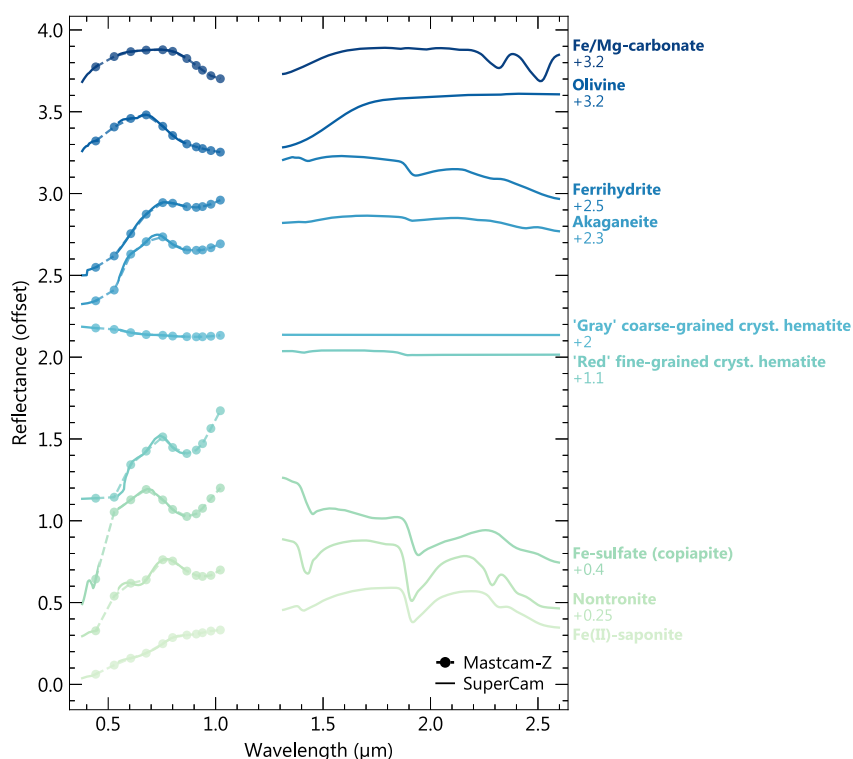
During the first 1.5 years of the mission, corresponding to the first ~420 sols (i.e., Martian days), the rover investigated two geological units of the crater floor: the Séítah and Mááz formations (Figure 1; Sun et al., 2023), both inferred to be igneous.

The Séítah formation is interpreted as an olivine-rich cumulate, containing both low and high-Ca pyroxenes, plagioclases, Cr-Fe-Ti oxides, phosphates, carbonates, phyllosilicates and sulfates (Beysac et al., 2023; Clavé et al., 2023; Farley et al., 2022; Liu et al., 2022; Mandon et al., 2023; Scheller et al., 2022; Wiens et al., 2022). In the visible and near-infrared (see Section 4), Séítah rocks show reflectance spectra with a deep 0.7–1.8  $\mu\text{m}$  absorption (minimum presumed to be between 1.0 and 1.3  $\mu\text{m}$ , where there is a gap in the spectral coverage of SuperCam, see Section 3.2) attributed to olivine (Horgan et al., 2023; Mandon et al., 2023; Rice et al., 2023; Figures 2–4). They also show moderate 0.53  $\mu\text{m}$  band depths (Rice et al., 2023; Horgan et al., 2023; Figure 4) and absorptions from small amounts of Fe<sup>3+</sup>-oxides such as hematite or the ferrihydrite suggested by Mandon et al. (2023). Typical spectra of Séítah rocks also show weak absorption features at 1.94, 2.33, and 2.39  $\mu\text{m}$  (Figure 3), which were attributed to small amounts of Mg-phyllsilicates (e.g., Mg-smectite, serpentine, talc and/or brucite; Mandon et al., 2023). Variability in the spectra was observed within and between targets, with additional weak absorptions at 2.23, 2.29, 2.47, and 2.53  $\mu\text{m}$ , indicative of an Al-OH and/or Si-OH-bearing phase (such as an Al-phyllsilicate and/or hydrated silica), Fe<sup>3+</sup>-phyllsilicates, akaganeite and carbonates, respectively (Mandon et al., 2023; Royer et al., 2023).

The overlying Mááz formation is interpreted to be lava flows and/or pyroclastic flows of basaltic composition, exhibiting elemental compositions and reflectance and Raman spectra that are consistent with the presence of Fe-rich augite, possibly ferrosilite and plagioclase, as well as Fe-Ti oxides, Si-rich phases, phyllosilicates, sulfates and perchlorates (Horgan et al., 2023; Scheller et al., 2022; Udry et al., 2023; Wiens et al., 2022). Rocks belonging to the Mááz formation have spectral reflectance signatures consistent with weakly altered and oxidized basalts. Typical rock spectra have moderate depth Fe-oxide absorptions at 0.53  $\mu\text{m}$ , a broad and shallow absorption at ~0.9  $\mu\text{m}$ , and weak 1.42, 1.93, 2.28, 2.39, and 2.46  $\mu\text{m}$  absorptions (Figures 3–5), consistent with a mixture of Fe<sup>3+</sup>-oxyhydroxides (ferrihydrite, akaganeite) and Fe<sup>3+</sup>-phyllsilicates (nontronite or hisingerite; Rice et al., 2023; Horgan et al., 2023; Mandon et al., 2023). In some rocks, an absorption centered near 0.86  $\mu\text{m}$  was observed (Figure 4), which suggested the presence of crystalline red hematite (Horgan et al., 2023; Rice et al., 2023). These spectral features contrast with those of the Séítah rocks, where the 2.3  $\mu\text{m}$  metal-OH feature shifts from ~2.33 to ~2.29  $\mu\text{m}$ . This indicates greater Fe<sup>3+</sup> relative to Mg in phyllsilicate mineral structures and indicates variation in carrier mineral and likely different redox states, which we examine further below and compare with spectra from the delta fan rocks.



**Figure 1.** (a) Photogeological map (Stack et al., 2020) overlain on HiRISE basemap. (b) Interpretative stratigraphic column of Jezero crater floor and fan areas (modified from Stack et al. (2024) and Ives et al. (2023)) color-coded by geologic members. Lateral extensions of members between the Cape Nukshak and Hawkswall Gap sections are demonstrated by Dehouck et al. (2023). (c–k) Mastcam-Z enhanced-color images (Red: 0.63  $\mu\text{m}$ , Green: 0.54  $\mu\text{m}$ , Blue: 0.48  $\mu\text{m}$ ) of selected outcrops of the main geological members discussed in this paper (acquired on sols: (c) 492; (d) 727; (e) 785; (f) 422; (g) 423; (h) 449; (i) 502; (j) 211; (k) 78). Spectra and images IDs and sols of acquisition are reported in Supporting Information S1.



**Figure 2.** Laboratory spectra of minerals of interest, convolved to Mastcam-Z and SuperCam spectral resolutions. Ferroan saponite (grain size <45 μm), nontronite (45–75 μm), copiapite (<25 μm), akaganeite (unknown grain size), olivine (Fo#60, grain size unknown) and Fe/Mg-carbonate (45–90 μm) spectra are from the RELAB library (Milliken, 2020) and from samples SA-EAC-059, JB-CMP-026-B, CC-JFM-013-A, JB-CMP-048, PO-RGB-045 and CB-EAC-003-B, respectively. Red (~0.012 μm) and gray hematite (500–1,000 μm) spectra are from samples HMS3 and WD39, respectively (Lane et al., 2002). Ferrihydrite (nanophase, grain size <45 μm) spectrum is from sample JB-498-A (Bishop & Murad, 2002).

For these two geological units, the Mastcam-Z and SuperCam VISIR were not previously analyzed conjointly, which would aid in the validation of mineralogical interpretation.

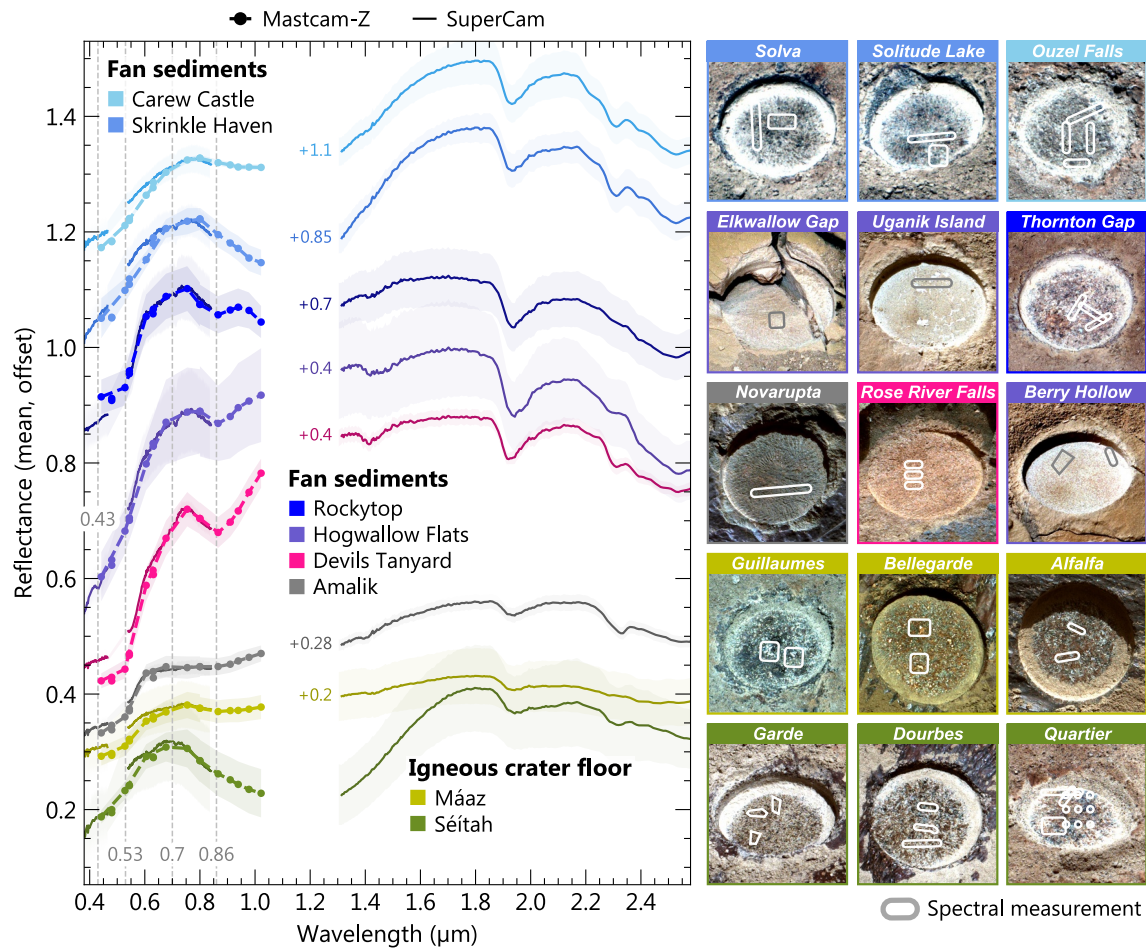
### 3. Data Set and Methods

#### 3.1. Target Selection and Main Geological Members Investigated

Within each main geological member (Figure 1b; for definitions, see Stack et al., 2024), we selected in-place bedrock targets, excluding float rocks and regolith, for which we have both SuperCam and Mastcam-Z coverage (unless specified otherwise). This selection includes natural surfaces as well as abraded rocks. Because the abraded rocks are freshly exposed surfaces and mostly devoid of dust particles and coatings, their associated spectra represent a clearer view of Fe mineralogy and redox conditions. Natural rock spectra are affected by the presence of variable amounts of coatings and airfall dust, which can induce albedo variation and ferric-related spectral features in the visible (e.g., Garczynski et al., 2022; Johnson et al., 2015) and decrease the contrast of spectral features associated with the substrate (Mandon et al., 2023). If a SuperCam Laser-Induced Breakdown Spectroscopy (LIBS) measurement was performed on these targets, the plasma shock wave reduced dust loading on the surface and associated spectral features in the VISIR.

For the crater floor units Máaz and Séítah (see Section 2), we analyzed the spectra from ~140 natural surface bedrock targets as well as six abraded patches (Figure 3) out of the seven performed. One abraded patch, target *Montpezat*, was significantly covered by tailings from the abrasion activity and was not considered.

Between sols ~420 and 700 of the mission (April 2022–February 2023), *Perseverance* explored sedimentary units near the front of the western delta fan, which are interpreted to be stratigraphically above the igneous Séítah and Máaz formations (Paige et al., 2024; Quantin-Nataf et al., 2023). The rocks exposed at this location are

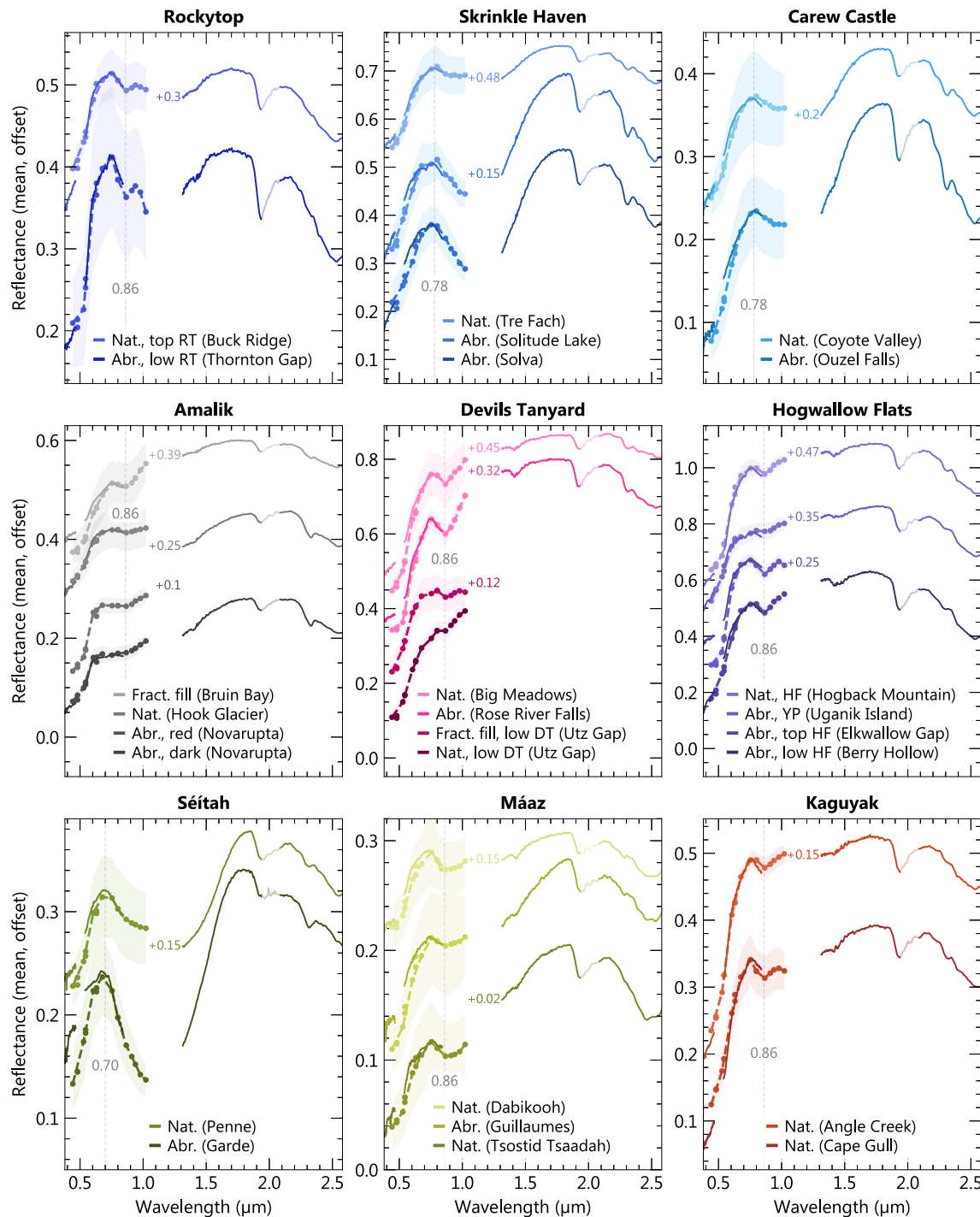


**Figure 3.** Mastcam-Z/SuperCam mean merged spectra of all rocks abraded until sol 803 along with location of SuperCam measurements and Mastcam-Z regions of interests used to produce the merged spectra, overlain on Mastcam-Z right eye images (enhanced colors, each stretched independently; Red: 0.63  $\mu\text{m}$ , Blue: 0.48  $\mu\text{m}$ ). Each abraded patch is about 5 cm in diameter. All Mastcam-Z spectra have been offset to match the SuperCam VIS spectra at 0.754  $\mu\text{m}$ . Low opacity envelopes around each spectrum represent standard deviations of Mastcam-Z regions of interest or SuperCam rasters. Spectra and images IDs and sols of acquisition are reported in Supporting Information S1.

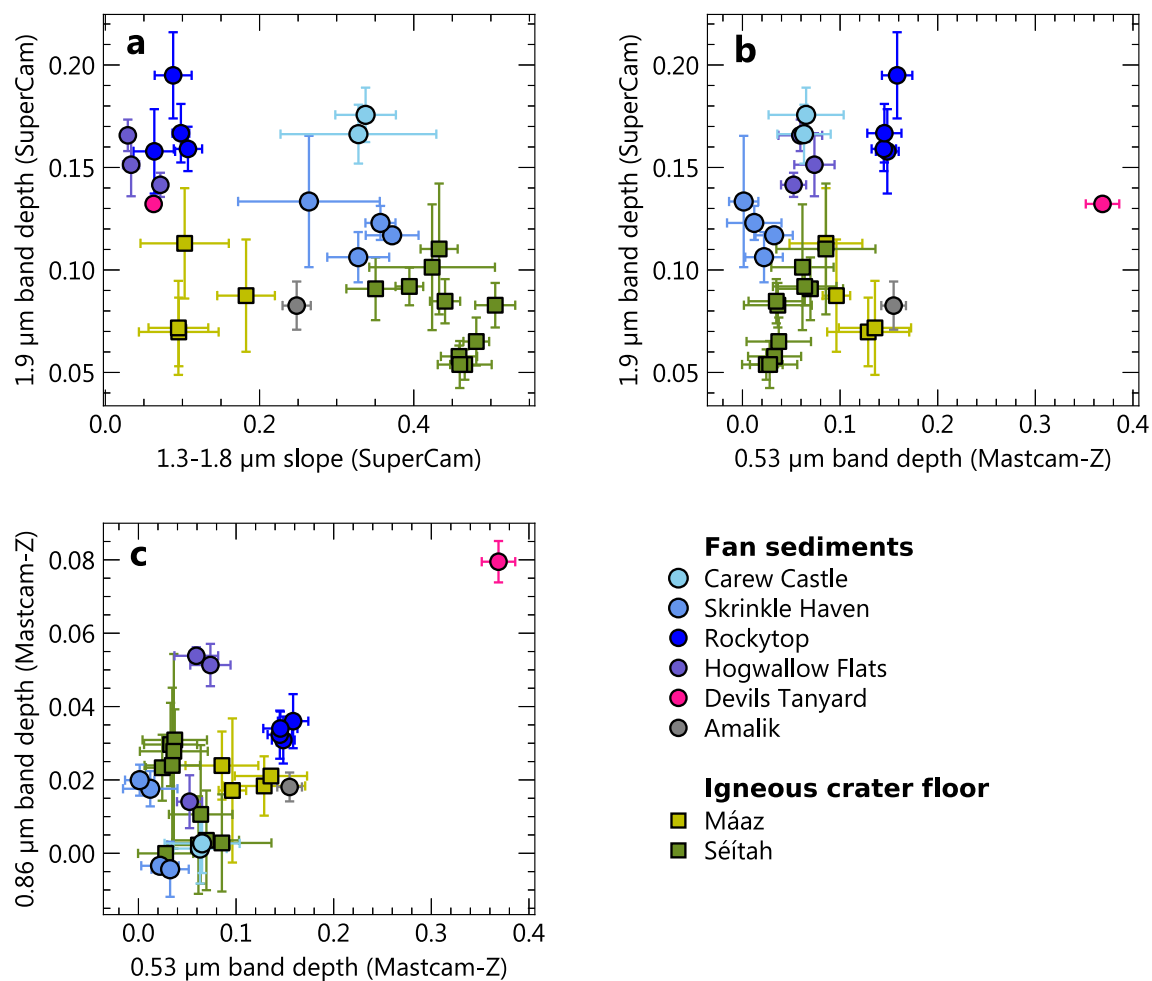
regrouped into the ~30 m-thick Shenandoah formation, which occurs in two stratigraphic sections: Cape Nukshak to the southwest and Hawksbill Gap to the northeast (Figure 1; Stack et al., 2024). At this location, we focused on units that are well exposed and for which we have sufficient data: in the Hawksbill Gap section, this includes the Devils Tanyard member (also regrouped with overlying Hughes River Gap strata), the Hogwallow Flats member, and the Rockytop member (Figure 1). The Boston Knob member, which was observed on sols 457–459 and 699–700, was excluded from our analysis because of uncertainty about whether it is in-place in the stratigraphy. In the Cape Nukshak section, we focused on the Kaguyak, Amalik, Knife Creek (lateral equivalent of Devils Tanyard; Dehouck et al., 2023; Stack et al., 2024), and Yori Pass (lateral equivalent of Hogwallow Flats; Dehouck et al., 2023; Stack et al., 2024) members (Figure 1). The Alagnak member was excluded due to lack of data. In the fan front area, one rock—estimated to be representative of the member—was abraded for each of the following members: Amalik, Devils Tanyard, Yori Pass and Rockytop (Figure 3). At Hogwallow Flats, one abrasion was performed at the bottom of the stratigraphy (target *Berry Hollow*) and one at the top (target *Elkwallow Gap*; Figure 3). Kaguyak is the only member of those investigated in this study at the fan front area that was not abraded. In the Devils Tanyard member, we also analyzed the spectra from one natural surface that was dust-cleaned by the gaseous Dust Removal Tool (gDRT) of the rover turret (target *Utz Gap*).

On sol 707, *Perseverance* began to ascend through the upper part of the exposed stratigraphy (Figure 1). From orbit, the top of the delta fan was grouped by Stack et al. (2020) into two main photogeological units: the “curvilinear unit,” characterized by decimeter scale sets of alternating light and dark layers that truncate against





**Figure 4.** Combined Mastcam-Z and SuperCam spectra of targets in the various members explored during the crater floor, fan front and top campaigns (Nat.: natural rock surface; Abr.: abraded rock surface; Fract. fill: fracture fill; DT: Devils Tanyard; HF: Hogwallow Flats; YP: Yori Pass; RT: Rockytop). The target names are indicated in brackets. Some Mastcam-Z observations of interest (e.g., *Utz Gap*) are not associated with any SuperCam spectra. Lower opacity spectra segments near 2  $\mu\text{m}$  correspond to the main atmospheric  $\text{CO}_2$  absorption range, where residuals might affect the spectra. All Mastcam-Z spectra have been offset to match the SuperCam VIS spectra at 0.754  $\mu\text{m}$ . Low opacity envelopes around each spectrum represent standard deviations of Mastcam-Z regions of interest or SuperCam rasters. Spectra IDs and sol of acquisition are reported in Supporting Information S1.



**Figure 5.** Mastcam-Z and SuperCam spectral parameters tracking the signature of hydration (1.9  $\mu\text{m}$  band depth), some  $\text{Fe}^{2+}$ -bearing phases such as olivines, carbonates, phyllosilicates or high-Ca pyroxenes (1.3–1.8  $\mu\text{m}$  slope),  $\text{Fe}^{3+}$  phases such as hematite and copiapites (0.86  $\mu\text{m}$  band depth) and  $\text{Fe}^{3+}$ -oxides (0.53  $\mu\text{m}$  band depth) in the abraded rock spectra measured at Jezero crater up to sol 803. Note that the 1.9  $\mu\text{m}$  band depth parameter is not (or weakly) sensitive to hydroxylated species with no structural  $\text{H}_2\text{O}$  molecule (e.g., brucite, serpentine). Formulation of the spectral parameters is described in Table 1. Error bars correspond to the standard deviation of parameters within one SuperCam raster or Mastcam-Z ROI.

each other, and the “blocky unit” that forms steep-sided, boulder-shedding elongate ridges. From the ground, two main types of facies were reported for in-place outcrops of the curvilinear unit, the Skrinkle Haven (Ives et al., 2023) and Carew Castle members. These members are overlain by a boulder-rich unit of float rocks (a likely expression of the blocky unit), not discussed further here. Among the bedrock targets analyzed in the fan top area until sol 800, three were abraded: two in the Skrinkle Haven member and one in the Carew Castle member at the Onahu outcrop (Figure 3). The Carew Castle rocks were first investigated from afar as distant buttes and then analyzed with proximity science at the Onahu outcrop. We limited our investigation to conclude with analysis of the Onahu outcrop (sol  $\sim$ 800 of the mission).

### 3.2. Reflectance Spectra

The rover payload does not include analytical techniques like X-ray Absorption Near Edge Structure (XANES) or Mössbauer spectroscopy that enable direct measurements of the redox states of specific elements. However, the Mastcam-Z and SuperCam instruments acquire relative reflectance measurements in the visible and near-infrared range (VISIR). At these wavelengths, electronic transitions related to Fe (e.g., crystal field transition, ligand-to-metal charge-transfer, intervalence charge transfer) induce absorption bands that are distinct in position, strength and width depending on whether Fe is present in a reduced/ferrous ( $\text{Fe}^{2+}$ ) or oxidized/ferric ( $\text{Fe}^{3+}$ ) form and its

**Table 1**

*Spectral Parameters Used in This Study, Computed as  $1 - R/R_c$  With  $R$  Being the Reflectance Measured at Band Center and  $R_c$  the Reflectance of the Continuum at Band Center*

Spectral parameter	Band center ( $\mu\text{m}$ )	Continuum anchors ( $\mu\text{m}$ )	Sensitivity
0.53 $\mu\text{m}$ band depth (Mastcam-Z)	0.528	0.441, 0.605	Fe <sup>3+</sup> -oxides
0.86 $\mu\text{m}$ band depth (Mastcam-Z)	0.866	0.801, 0.940	Fine-grained crystalline hematite, copiapite group (Low Ca-pyroxenes and other ferric sulfates can also raise moderately positive values)
1.9 $\mu\text{m}$ band depth (SuperCam)	1.937	1.851, 2.107	H <sub>2</sub> O
1.3–1.8 $\mu\text{m}$ slope (SuperCam)	1.326	1.807 (flat continuum)	Fe <sup>2+</sup> (strongly positive for olivine, high Ca-pyroxenes and some other ferrous phases (e. g., Fe <sup>2+</sup> -bearing carbonates or Fe <sup>2+</sup> -bearing phyllosilicates)), moderately positive for ferric minerals

coordination in the mineral structure (e.g., Figure 2). The ferric-related electronic absorptions occur in the  $\sim 0.2$ – $1.2 \mu\text{m}$  range and include strong charge transfer absorptions in the UV-Vis wavelengths ( $< \sim 0.7 \mu\text{m}$ ), while the ferrous-related absorptions are mainly observed  $> \sim 0.7 \mu\text{m}$ .

SuperCam's VIS point spectrometer (Maurice et al., 2021; Wiens et al., 2020) measures reflected light from 0.39 to 0.47  $\mu\text{m}$  (via a crossed Czerny-Turner spectrometer) and 0.54–0.85  $\mu\text{m}$  (via a transmission spectrometer). The Infrared Spectrometer (IRS; Fouchet et al., 2022) acquires spectra from 1.3 to 2.6  $\mu\text{m}$ , enabling the identification of a wide variety of minerals, including mafic igneous minerals and secondary phases such as phyllosilicates, sulfates, or carbonates (Dehouck et al., 2023; Fouchet et al., 2022; Mandon et al., 2023; Maurice et al., 2021; Wiens et al., 2020). Mastcam-Z provides multispectral stereo-imaging with 12 narrowband filters centered in the 0.44–1.02  $\mu\text{m}$  range, longer than the spectral VIS range of SuperCam and sensitive to longer-wavelength regions associated with more Fe-related absorptions (Bell et al., 2021). These two instruments are thus highly complementary for identifying the Fe-related VISIR absorptions and understanding the associations of different oxides. For example, the main band of hematite at 0.86  $\mu\text{m}$  sampled only by Mastcam-Z, and the olivine and pyroxene absorption bands cannot be fully covered by SuperCam alone. By contrast, SuperCam is highly sensitive to hydrous/hydroxylated minerals and able to detect narrow electronic absorptions by virtue of a greater spectral resolution than Mastcam-Z (Fouchet et al., 2022; Mandon et al., 2023).

We used the data measured by the two instruments, calibrated to relative reflectance—the flux reflected by a target to that which would be reflected by a Lambertian surface illuminated under the same geometry—using pre-flight measurements and observations of the Mastcam-Z and SuperCam calibration targets (processing described in details in Mandon et al. (2023), Merusi et al. (2022), and Royer et al. (2023)). While including calibration targets in the processing mitigates atmospheric influence on the spectra of near-field targets, additional correction is performed on the IRS spectra using an atmospheric model whose parameters are empirically set to minimize atmospheric-related absorptions (Royer et al., 2023).

The spatial resolutions of the instruments vary, with the VIS field-of-view (FOV) sampling at 0.74 mrad ( $\sim 2.2 \text{ mm}$  at 3 m distance), and the IRS at 1.15 mrad ( $\sim 3.5 \text{ mm}$  at 3 m). Mastcam-Z images acquired here were typically taken at 110 mm focal length, corresponding to 0.067 mrad ( $\sim 0.2 \text{ mm/pixel}$  at 3 m). The effective spatial resolution of the Mastcam-Z measurements depended on the number of pixels selected and averaged for a given region of interest (ROI).

For every combined observation of the same rock targets by the two instruments, we computed a mean spectrum of the SuperCam measurement (consisting of a raster of one to 10 points) and extracted from the corresponding Mastcam-Z image an average spectrum from a co-located region of interest, resulting in similar spatial coverage for comparison between the two instruments. As part of the standard Mastcam-Z data analysis, spectra from the left and right eyes cameras were scaled to their common 800 nm filters (Bell et al., 2021).

Discrepancies between the two instruments sometimes persisted due to residual photometric effects owing to variable shadowing and/or acquisition times and distinct dust cover depending on whether the Mastcam-Z activity was performed before or after partial dust removal by a SuperCam's LIBS activity (Johnson et al., 2022). Although the spectral shapes were similar in most observations, an offset in reflectance was sometimes observed.

Here, we focus on spectral shapes rather than absolute reflectance: in the spectra shown here, Mastcam-Z data were normalized to SuperCam spectra at 0.754  $\mu\text{m}$  (the center of one of the Mastcam-Z left eye filters). To assess the variability of different  $\text{Fe}^{2+}$ ,  $\text{Fe}^{3+}$ -bearing phases as well as hydration in the stratigraphy, we computed spectral parameters, with formulation and sensitivity detailed in Table 1.

### 3.3. Comparison to Pancam and Mastcam Data

To gain perspective on the redox conditions recorded in Jezero bedrock, we compare member spectra measured by Mastcam-Z with the primary MER Pancam and MSL Mastcam spectral classes identified at other Mars landing sites (Farrand et al., 2008, 2013, 2014, 2016; Rice et al., 2022). Furthermore, since the instrument payloads of the other rovers include additional analytical techniques to investigate the Fe mineralogy and distinguish between  $\text{Fe}^{2+}$  and  $\text{Fe}^{3+}$  phases, comparison of spectra allows bridging datasets to gain more insight into the Jezero rocks. Each of the MER rovers was equipped with a Mössbauer spectrometer, which allowed quantification of the Fe mineralogy and redox state (e.g., Morris et al., 2006a, 2006b), and the *Curiosity* rover had X-ray diffraction for mineral determination of crystalline materials, which in many cases, was sensitive to Fe oxidation state (e.g., Bristow et al., 2018; Rampe, Bristow, et al., 2020; Treiman et al., 2016).

Because Pancam, Mastcam and Mastcam-Z spectra have different spectral bandpasses (Bell et al., 2003, 2017, 2021), their calibrations may subtly differ, and the degree and nature of surface preparation varies, all of which encourage caution when comparing among these datasets. The freshest surfaces analyzed by Mastcam on *Curiosity* were brushed rocks, some of which included residual fines or coatings. Rocks abraded and brushed by the Rock Abrasion Tool (RAT) onboard the MER rovers varied in the amount of residual drill tailings on their surfaces, compared to rocks abraded by *Perseverance's* tool and subjected to gDRT cleaning (e.g., Zorn et al., 2023).

## 4. Results

### 4.1. Crater Floor Igneous Rocks

By merging spectra from the *Perseverance* instruments, the broad absorption band consistent with olivine on its left wing in Mastcam-Z data and on its right wing in SuperCam IRS data in Séítah is inferred, with a minimum between 1.0 and 1.3  $\mu\text{m}$ , within the spectral gap between the two datasets (Figure 4), consistent with prior Séítah studies (Section 2).

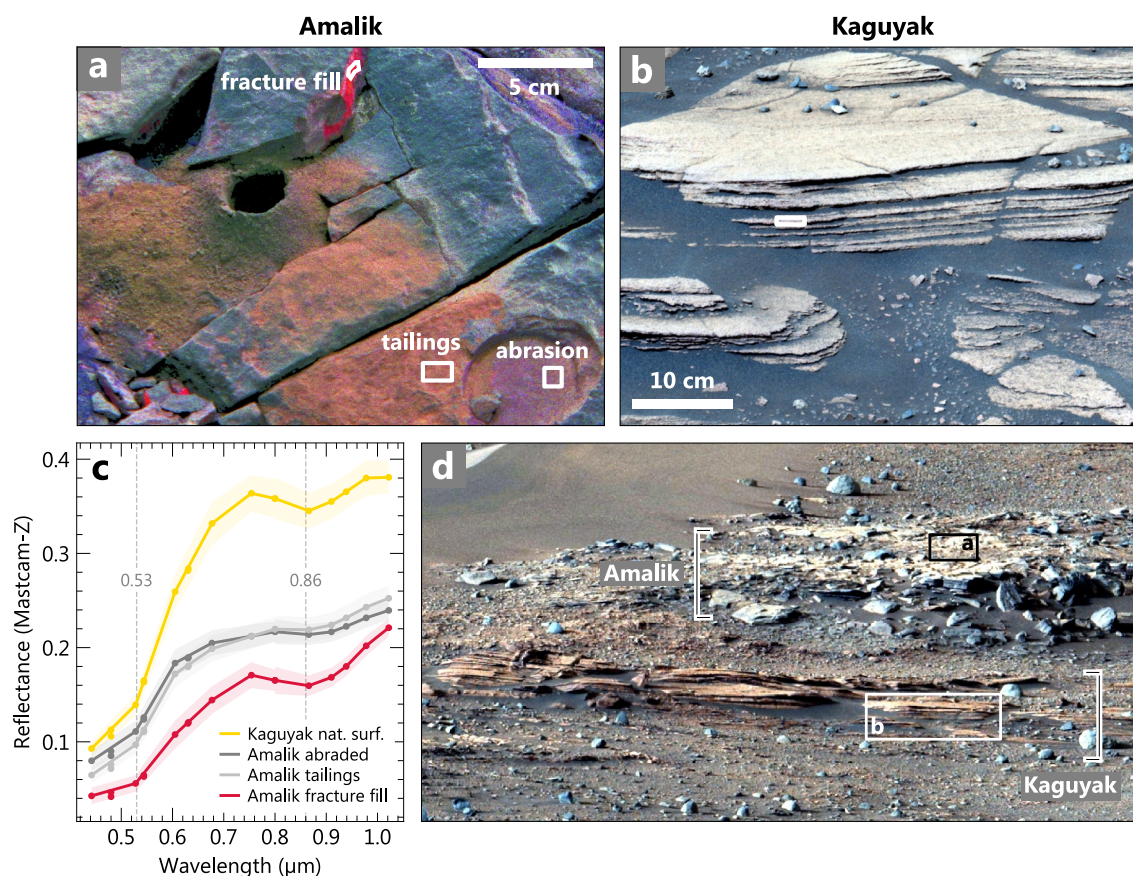
For Mááz, it was hypothesized that low-Ca pyroxenes could be responsible for the 0.9  $\mu\text{m}$  absorption observed in the Mastcam-Z data (Horgan et al., 2023). Investigation of the merged SuperCam-Mastcam-Z spectra in this work reveals that the spectra of targets exhibiting this absorption do not show a broad absorption near 2  $\mu\text{m}$  that could be indicative of pyroxene being the prime species responsible for the 0.9  $\mu\text{m}$  band (Figure 4). Instead, typical merged spectra of Mááz show absorptions near 0.53  $\mu\text{m}$  and a strong red slope in the 0.9–1.8  $\mu\text{m}$  as well as a broader 1.9  $\mu\text{m}$  band (Figure 4), previously noted as typical of oxyhydroxides such as ferrihydrite or akaganeite (Mandon et al., 2023).

Figure 5 shows the spectral parameters listed in Table 1 that were computed using the Mastcam-Z and SuperCam spectra of abraded rocks to evaluate the contributions of  $\text{H}_2\text{O}$ , some ferrous materials, and ferric oxides on the spectra. Broad trends are observed within the igneous rocks of the crater floor that were abraded: surfaces with the strongest  $\text{H}_2\text{O}$  absorptions are associated with the strongest  $\text{Fe}^{3+}$ -oxides signatures and the weakest  $\text{Fe}^{2+}$  signatures. This suggests that the hydrous alteration was associated with oxidation of the rocks and alteration of the primary grains.

### 4.2. Sediments of the Western Fan

#### 4.2.1. Kaguyak Member

The base of the Cape Nukshak stratigraphy corresponds to the Kaguyak member (Figure 1), which is composed of sandstones with planar, horizontal to sub-horizontal lamination (Stack et al., 2024). Observations of the rocks within the Kaguyak member are scarce, and no abrasion was performed. Though they are relatively covered by dust, strata of the Kaguyak member exhibit a reddish hue that is distinct from typical surfaces coated by thick dust (Figure 6d) and instead indicates oxidized materials in the bedrock. Indeed, reflectance spectra of targets that were partially cleared of dust by LIBS (targets *Angle Creek* and *Cape Gull*) show a moderate red slope in the 1.3–



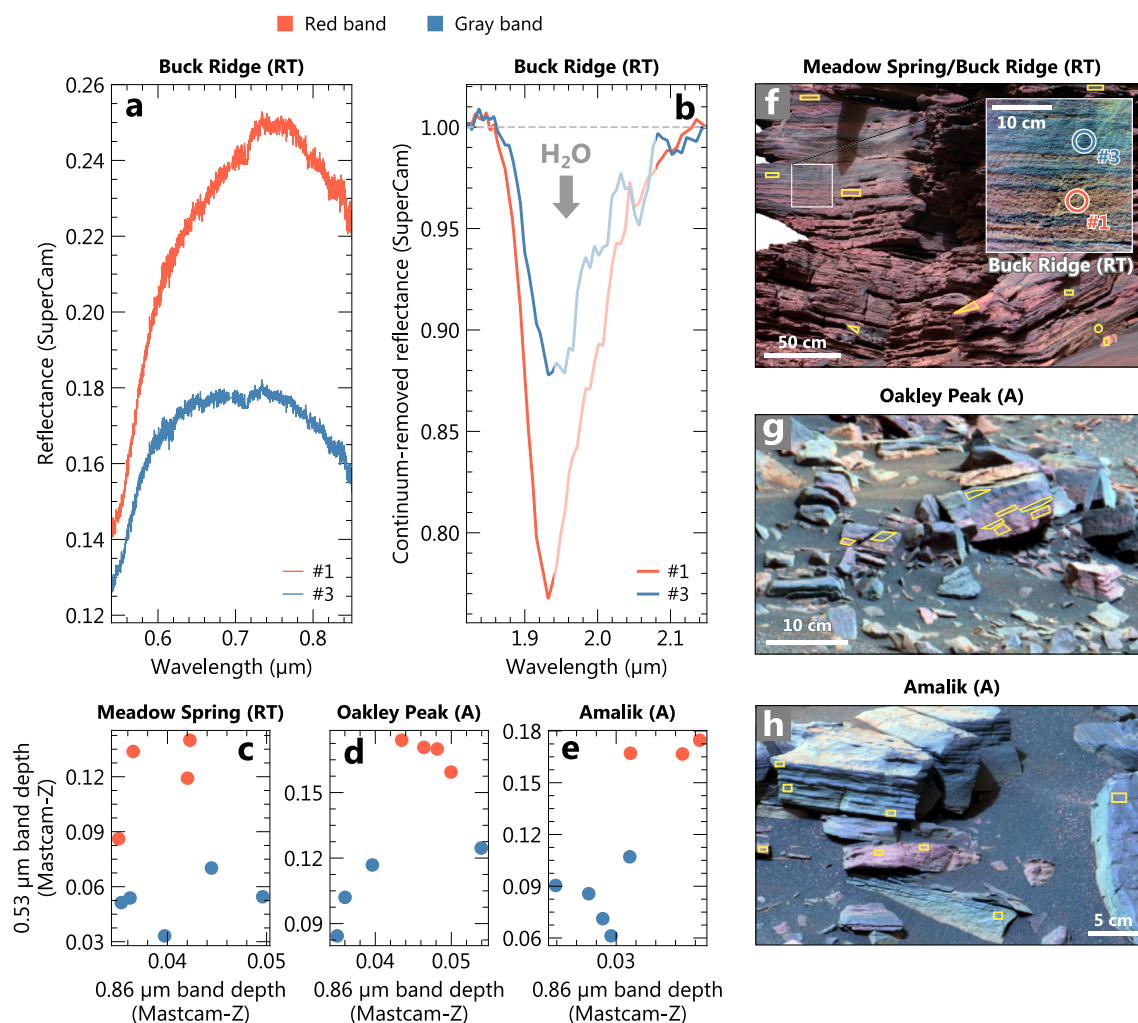
**Figure 6.** (a) Mastcam-Z Decorrelation Stretch (DCS; Rice et al., 2023) right eye image (Red: 1.02 μm, Green: 0.91 μm, Blue: 0.80 μm) showing enhanced hematite signature in fuchsia hue. (b) Mastcam-Z enhanced-color left eye image (Red: 0.63 μm, Green: 0.54 μm, Blue: 0.48 μm). (c) Mastcam-Z spectra showing enhanced hematite-related absorptions near 0.53 and 0.86 μm at Kaguyak and on a fracture-fill at Amalik. Low opacity envelopes around each spectrum represent standard deviations of Mastcam-Z regions of interest. Corresponding locations of spectra are shown in (a) and (b). (d) Portion of a Mastcam-Z mosaic taken on sol 420 and showing the Amalik and Kaguyak members. Images IDs and sol of acquisition are reported in Supporting Information S1.

1.8 μm range (Figure 4), which is consistent with low  $\text{Fe}^{2+}$ , as well as a V-shaped absorption centered at 0.86 μm and indicative of fine-grained red hematite (Figures 4 and 6c). This signature of oxidation contrasts with the spectra of the overlying strata of the Amalik member, described hereafter.

#### 4.2.2. Amalik Member

The rocks at Kaguyak are overlain by coarse siltstones of the Amalik member, which also show planar, horizontal to sub-horizontal lamination (Stack et al., 2024). Amalik rocks exhibit banding of alternating gray and red materials (Figures 7g and 7h). The gray intervals are overall dark in the visible (relative reflectance <0.2). In the infrared spectrum, Amalik data show a relatively strong slope in the 0.8–1.8 μm range suggesting some ferrous materials such as olivine,  $\text{Fe}^{2+}$ -bearing carbonates and/or  $\text{Fe}^{2+}$ -bearing phyllosilicates (Figures 3 and 4). The mean spectrum of the abraded patch (mostly free of dust) has a moderate 0.53 μm absorption in line with the abraded patches of the fan front area rocks, but a weaker 0.86 μm absorption (Figure 3), implying the presence of some  $\text{Fe}^{3+}$ -oxides but limited crystalline red hematite.

The darkening and decrease of the overall spectral slope in the visible compared to the rest of the dataset might indicate the presence of a fine-grained, strong visible absorber such as opaque minerals like Fe-sulfides or oxides like magnetite, coarse-grained gray hematite, ilmenite or chromite, which tend to reduce the reflectance levels (Loeffler & Prince, 2022). We note that darkening on the order of tens % of reflectance can be achieved with only a few wt.% of these minerals (Loeffler & Prince, 2022), which would be below the LIBS detection thresholds of S in sulfides. Potential Ti or Cr-magnetite are reported by Mansbach et al. (2023) at Jezero from analysis of the



**Figure 7.** Color banding at Amalik and Rockytop. (a) SuperCam visible spectra measured on a dark and red band at Rockytop (location in (f)). (b) SuperCam continuum-removed spectra in the H<sub>2</sub>O absorption range measured on a dark and red band at Rockytop (location in (f)). (c–e) Mastcam-Z 0.53 and 0.86 μm band depths of regions of interest (locations in (f–h)). (f–h) Mastcam-Z enhanced-color left eye images (Red: 0.75 μm, Green: 0.53 μm, Blue: 0.44 μm) at Amalik (A) and Rockytop (RT). The inset of the Meadow Sprint outcrop corresponds to a SuperCam RMI image of the *Buck Ridge* target, with the location of the SuperCam VISIR measurement plotted in (a, b). Spectra and images IDs and sol of acquisition are reported in Supporting Information S1.

Planetary Instrument for X-ray Lithochemistry (PIXL) but do not seem to be significantly more abundant at Amalik; no sulfides are reported by Mansbach et al. (2023).

The average Amalik spectrum in Figure 3 also shows weaker slopes in the 0.5–0.6 μm and 0.6–0.9 μm ranges compared to the crater floor and other deltaic rocks that form an unusual “step” feature in the spectra at ~0.6 μm (Figure 3). While the presence of any of these darkening agents is expected to broadly decrease the reflectance levels over the spectral range investigated, none of these agents fully explain the 0.6 μm “step” feature. Various minerals can display similar spectral features (e.g., Clark et al., 1990) due to strong absorption centered in the UV and extending in the visible, and caused by electronic transitions. The presence of Mg-rich serpentine at Amalik has been proposed by Dehouck et al. (2023); Fe-poor serpentines such as chrysotile and lizardite can exhibit a step feature near 0.6 μm (e.g., Clark et al., 1990), likely caused by Si-O charge transfer and/or Fe contamination and that could account for our observation. Another possibility would be the presence of a phase with a conduction band, which is typically observed in the case of semi-conductor elements (such as sulfur). This type of electronic process produces strong absorption in the UV-VIS range, causing the spectrum to approximately look like a step function (e.g., Clarke, 1999). As with the oxides and sulfides, these types of absorption are strong and do not

require a significant amount of the associated phase to appear, but their presence or absence at Amalik cannot be definitively determined.

The third distinctive aspect of Amalik is its banding. The spectral differences between the gray and the red bands in the rocks are subtle, but the red bands absorb more deeply at 0.53  $\mu\text{m}$  (Figure 7), indicative of more elevated  $\text{Fe}^{3+}$ -oxide contents and/or different grain sizes. Both types of materials show weak absorptions near 0.86  $\mu\text{m}$  of comparable depths, implying that ferric materials such as crystalline red hematite are not restricted to the red bands but are present in both types (Figure 7).

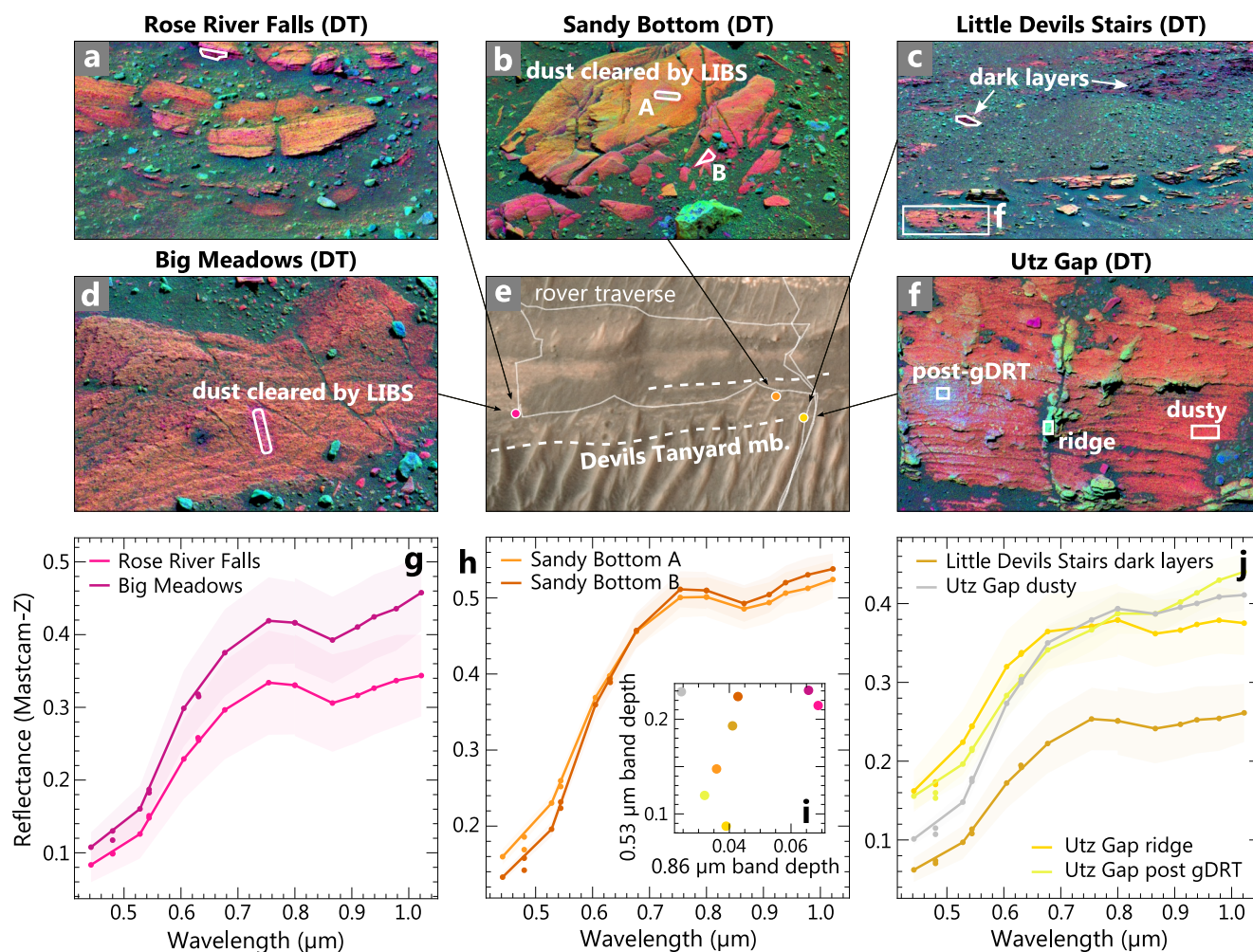
The abrasion performed at Amalik (target *Novarupta*) exhibits a rough surface, with the dark gray materials in positive relief compared to the redder materials in negative relief (Figure 3), possibly implying that the abrasion stopped near an interface of red and gray bands. Another possibility is the presence of fines derived from coarse-grained gray hematite, which would typically exhibit a red color, although gray hematite has not been readily detected at this location. Unfortunately, the sole raster performed by SuperCam on this abraded target includes only dark areas, which precludes a SuperCam comparison between the two types of materials on the abraded patch. The spectral features of the gray areas are similar to the gray bands of non-abraded rocks at Amalik (i.e., weak red slopes in the visible, red slope between 0.8 and 1.8  $\mu\text{m}$ , moderate 1.9  $\mu\text{m}$  absorption depth compared to other rocks of the delta front, and sharp 2.33  $\mu\text{m}$  absorption; Figure 3). Mastcam-Z observations of the abraded patch show that, similar to the non-abraded Amalik rocks, the red areas exhibit visible spectra comparable to the gray areas but have slightly enhanced 0.53  $\mu\text{m}$  absorption pointing toward higher content and/or finer grain size of  $\text{Fe}^{3+}$ -oxides (Figure 4).

During the first coring activity at Amalik, portions of the rock slab broke and exposed reddish material, associated with deep 0.53 and 0.86  $\mu\text{m}$  absorptions, as well as a narrow peak reflectance position in the visible, consistent with fine-grained crystalline red hematite (target *Bruin Bay*; Figure 6). Given the fact that these spectral features are not observed on the tailings of the nearby cored surface, these materials might represent fracture-filling of a different, more ferric nature than the bedrock that preferentially broke along this plane during coring.

#### 4.2.3. Devils Tanyard/Hughes River Gap/Knife Creek Member

The base of the Hawksbill Gap stratigraphy corresponds to the Devils Tanyard member and overlying Hughes River Gap strata (Figure 1), which consist of planar laminated sandstones of variable exposure. Here, the outcrops share morphological and spectral features with the Knife Creek member (located right above Amalik) and hence have been interpreted as its lateral equivalent in the Cape Nukshak section (Dehouck et al., 2023; Stack et al., 2024). Abrasion of a Devils Tanyard rock (target *Rose River Falls*) shows the strongest oxidation of Fe features: the rock is redder than the other abraded members, has narrower reflectance peaks in the visible, and deeper 0.53 and 0.86  $\mu\text{m}$  absorptions, indicative of fine-grained crystalline hematite (Figures 3 and 5). The associated SuperCam spectrum is broadly flat in the 1.3–1.8  $\mu\text{m}$  range, suggesting a low contribution from the ferrous materials (Figures 3 and 5).

While the non-abraded bedrock at the location of *Rose River Falls* shares the spectral features described above (e.g., target *Big Meadows*; Figures 4 and 8), the apparent oxidation is not homogeneous throughout the unit, with variability in both the 0.53 and 0.86  $\mu\text{m}$  absorption strengths and the color of the bedrock in the DCS images with the 0.754, 0.528, and 0.442  $\mu\text{m}$  filters (Figure 8). Rocks in the vicinity of *Sandy Bottom*, East to *Rose River Falls*, show weaker 0.86  $\mu\text{m}$  absorption (Figure 8). *Utz Gap*, a bedrock target at the base of the Devils Tanyard member with raised, mineralized fractures, was cleared of dust using the gDRT of the rover turret. Here, no SuperCam VISIR observation was performed, but multispectral Mastcam-Z images were acquired. Interestingly, the cleared bedrock does not appear pink on the DCS images with the 0.754, 0.528, and 0.442  $\mu\text{m}$  filters, as opposed to other targets of the Devils Tanyard member (Figure 8) and shows weaker 0.53 and 0.86  $\mu\text{m}$  absorptions (Figures 4 and 8); all of these observations are consistent with less fine-grained hematite or of different grain size/crystallinity. This possibly indicates that fine-grained crystalline hematite formed heterogeneously through the Devils Tanyard member. We note that the bedrock cropping out at *Utz Gap* is at least  $\sim 2$  m below all other rock targets at Devils Tanyard; another possibility to explain the variability of  $\text{Fe}^{3+}$ -oxides is that this outcrop does not belong to the Devils Tanyard member. Near *Utz Gap* and at other locations, poorly outcropping rocks of the Devils Tanyard member alternate with dark-toned, thinly layered, deformed strata (such as at *Little Devils Stairs*), commonly purple to pink in the DCS images with the 0.754, 0.528, and 0.442  $\mu\text{m}$  filters (Figure 8c) and associated with 0.53 and 0.86  $\mu\text{m}$  absorption band depths intermediate to the *Rose River Falls* and *Utz Gap* outcrops (Figure 8i). These



**Figure 8.** (a, b, c, d, f) Mastcam-Z Decorrelation Stretch (DCS; Rice et al., 2023) left eye images (Red: 0.754  $\mu\text{m}$ , Green: 0.528  $\mu\text{m}$ , Blue: 0.442  $\mu\text{m}$ ) of selected outcrops in the Devils Tanyard (DT) member. In these color composites, dusty surfaces appear orange to red and more strongly oxidized surfaces appear pink (although details in DCS images are scene-dependent). The outcrop shown in (a) was captured before abrasion of the *Rose River Falls* target. (e) HIRISE basemap with corresponding locations of observations shown in other panels. (g, h, j) Mastcam-Z spectra extracted from regions of interest shown in white in (a–d and f). Low opacity envelopes around each spectrum represent standard deviations of Mastcam-Z regions of interest. (i) Mastcam-Z 0.53 and 0.86  $\mu\text{m}$  band depths of spectra shown in (g, h, j). Images IDs and sol of acquisition are reported in Supporting Information S1.

features are similar in morphology to mottled strata described by Broz et al. (2024) in the Hogwallow Flats member, which also exhibit  $\text{Fe}^{3+}$ -oxides signatures in the Mastcam-Z data.

#### 4.2.4. Hogwallow Flats/Yori Pass Member

The Hogwallow Flats member is stratigraphically above the Hughes River Gap member in the Hawksbill Gap section and extends in the Cape Nukshak section at Yori Pass (Figure 1). These rocks consist of siltstones and are the finest-grained materials observed by the rover at the delta front (Figure 3; Stack et al., 2024). The combined Mastcam-Z/SuperCam spectra measured in this member have the weakest red slope in the 1.3–1.8  $\mu\text{m}$  range, suggesting limited  $\text{Fe}^{2+}$  content in the bulk rock.

A strong absorption is observed near 0.86  $\mu\text{m}$  (Figures 3–5). The 0.53  $\mu\text{m}$  band depth is usually weak, likely indicating that red hematite is not a major spectral contributor (Figures 3–5). SuperCam spectra exhibit a narrow absorption at 0.43  $\mu\text{m}$  (Figure 3). These spectral properties are consistent with  $\text{Fe}^{3+}$ -sulfates, which have absorptions centered near  $\sim 0.9 \mu\text{m}$  and at 0.43  $\mu\text{m}$ , but do not absorb near 0.53  $\mu\text{m}$  (e.g., Cloutis et al., 2006). The narrow absorption at 0.43  $\mu\text{m}$  is an electronic transition of ions in hydroxyl-bridged  $\text{Fe}^{3+}$  sheets and the 0.43  $\mu\text{m}$  position in  $\text{Fe}^{3+}$ -sulfates is distinct from a similar 0.48  $\mu\text{m}$  absorption observed in  $\text{Fe}^{3+}$ -smectites (Fox



et al., 2021; Hunt & Ashley, 1979; Johnson et al., 2016). The  $\sim 0.9 \mu\text{m}$  absorption of copiapite minerals is centered at  $\sim 0.85\text{--}0.87 \mu\text{m}$  (Kong et al., 2011), while other  $\text{Fe}^{3+}$ -sulfates absorb at different wavelengths, with a band centered  $>0.90 \mu\text{m}$  in jarosite or  $\sim 0.80 \mu\text{m}$  in fibroferrite (e.g., Cloutis et al., 2006), making copiapites a preferred interpretation of the spectral features seen in Hogwallow Flats/Yori Pass spectra. This family of sulfates has 20 stoichiometric  $\text{H}_2\text{O}$ , which might be challenging to stabilize in present Martian surface dry conditions. Dehydration experiments (e.g., Liu & Wang, 2015; Turenne et al., 2022; Wang & Ling, 2011) show that copiapites can remain stable for years in low humidity environments, that they can retain the narrow  $\sim 0.43 \mu\text{m}$  and broad  $\sim 0.86 \mu\text{m}$  absorptions even when converted to less hydrated phases, and that they are good buffers for relative humidity. Wang and Ling (2011) concluded that they can remain stable in the very near Martian subsurface. Hence, these phases can be present on the surface if exposed recently, and copiapites (or products derived from dehydration and showing similar spectral features) are still reasonable matches for the spectral features observed on Hogwallow Flats rocks, especially considering the fine grain size of Hogwallow Flats siltstones, which could have promoted erosion.

From one abraded patch to another, the spectra are variable in the visible range. The abraded top of Hogwallow Flats (target *Elkwallow Gap*) is redder and shows enhanced  $0.53$  and  $0.86 \mu\text{m}$  absorptions compared to the abraded base of the member (target *Berry Hollow*), consistent with  $\text{Fe}^{3+}$ -oxides variability within the Hogwallow Flats member. The abraded patch of the Yori Pass location (target *Uganik Island*) exhibits a weaker  $0.86 \mu\text{m}$  absorption compared to Hogwallow Flats (Figure 4), possibly due to increased Fe-free anhydrite veinlet content in the rock (Nachon et al., 2023).

#### 4.2.5. Rockytop Member

The Rockytop member sits stratigraphically above Hogwallow Flats. It is composed of pebbly sandstones that are cross-bedded in the lowest portions and exhibit planar stratifications in the upper ones. The spectra measured on rocks of the Rockytop member exhibit a broad and shallow absorption between  $0.7$  and  $1.7 \mu\text{m}$  (Figure 4), pointing toward the presence of ferrous component(s), likely a combination of the olivine clasts and Fe/Mg-carbonates detected by Hurowitz et al. (2023), Dehouck et al. (2023) and Phua et al. (2024). Crystalline red hematite is likely present in the Rockytop member, as indicated by elevated  $0.53$  and  $0.86 \mu\text{m}$  absorptions in the spectra of the abraded patch (target *Thornton Gap*). However, these bands are weaker than at Devils Tanyard, suggesting a variability in  $\text{Fe}^{3+}$ -oxide content and/or grain size (Figures 3 and 5).

Similar to Amalik, the planar stratified beds in the upper section of Rockytop show alternating strata of red and gray color (Figure 7f), with the gray layers being raised compared to the red ones. As for Amalik, the subtle difference between the two materials is that red bands have a narrower peak of reflectance in the visible and have stronger  $0.53 \mu\text{m}$  absorption, consistent with  $\text{Fe}^{3+}$ -oxides content and/or grain size variability. They are also associated with a deeper  $1.93 \mu\text{m}$   $\text{H}_2\text{O}$  absorption (Figure 7). At target *Buck Ridge*, a five point raster, there is a very good linear correlation ( $R^2 = 0.98$ ) between the  $0.53 \mu\text{m}$  ( $\text{Fe}^{3+}$ -oxides) and  $1.93 \mu\text{m}$  ( $\text{H}_2\text{O}$ ) band depths (Figure S1 in Supporting Information S1). The strength of the  $0.86 \mu\text{m}$  absorption is similar for the two types of bands, indicating, as for Amalik, no increased influence from crystalline hematite in the red bands.

#### 4.2.6. Skrinkle Haven and Carew Castle Members

The Skrinkle Haven member, which crops out over most of the traverse on the top of the fan, is composed of alternating recessive and resistant beds of light-toned rocks (Figure 1d). These beds are steeply dipping ( $>20^\circ$ ), often curved, and are composed of sandstones and pebbly conglomerates (Ives et al., 2023). The Carew Castle member, which is stratigraphically above the Skrinkle Haven member, crops out at fewer and more restricted locations around the rover traverse. It consists of alternating planar and cross-bedded strata of coarse sandstones to pebbly/cobbly conglomerates (Figure 1e).

The rocks of Skrinkle Haven and Carew Castle, despite exhibiting different sedimentary facies and grain sizes, have similar spectra in the visible and near-infrared. They are associated with an inferred broad  $\text{Fe}^{2+}$  absorption centered between  $1.0$  and  $1.3 \mu\text{m}$ , of strength similar to spectra of the Séítah formation (Figures 3–5). However, unlike Séítah, the reflectance peak in the visible (i.e., the left shoulder of the  $\text{Fe}^{2+}$  absorption) is positioned at longer wavelengths. While some olivine may have reflectance peaks centered near  $0.75 \mu\text{m}$  depending on Mg# and grain size, most pristine olivine spectra have peaks centered at lower wavelengths (e.g., Figure 2; Lapo et al., 2024). Carbonates with Fe in their structure are typically associated with peaks centered longward of

0.75  $\mu\text{m}$ , which likely explains the position of the peak in the spectra of the Skrinkle Haven and Carew Castle rocks. This is also consistent with the strong signature of carbonates measured by SuperCam IRS and other instruments in the Skrinkle Haven member (Dehouck et al., 2023; Hurowitz et al., 2023; Phua et al., 2024).

Both natural surfaces and abraded rocks of the Skrinkle Haven member show little to no oxidation signature: the 0.53  $\mu\text{m}$  absorption band is not always detected and when observed is very weak (typically <5% relative to the continuum). Furthermore, there is no to very weak 0.86  $\mu\text{m}$  feature (Figures 3–5). The Onahu outcrop from the Carew Castle member is associated with stronger  $\text{H}_2\text{O}$  absorption (Figure 5). It also seems slightly more oxidized with a marginally increased 0.53  $\mu\text{m}$  band depth compared to Skrinkle Haven but remains consistent with rocks being overall weakly oxidized (Figure 5).

## 5. Discussion

The nature and abundance of  $\text{Fe}^{3+}$  and  $\text{Fe}^{2+}$ -bearing minerals are variable at Jezero crater. We observe three types of variability: variability between the igneous floor units and fan unit strata, variability between members of the fan sedimentary rocks, and variability at smaller spatial scales within members, especially with cm-scale color banding at Amalik and Rockytop.

In the following sections, we first summarize the inter-units and member variability, and compare the signature of these members to the main spectral endmembers identified from previous rover exploration at other landing sites. We then propose scenarios for the origin of the small-scale color banding observed at Amalik and Rockytop, and finally discuss how the broad variability observed in our dataset fits into the history and properties of the Jezero system.

### 5.1. Variability of Fe Mineralogy at Jezero

#### 5.1.1. Variability of Fe Oxidation Between the Igneous Floor and the Western Fan

Strata of the fan front typically show stronger signatures of  $\text{Fe}^{3+}$ -bearing species compared to the igneous floor (Figures 3–5). While small amounts of poorly crystalline  $\text{Fe}^{3+}$ -oxyhydroxides and  $\text{Fe}^{3+}$ -phyllosilicates are associated with the floor units (Mandon et al., 2023), more significant signatures of crystalline  $\text{Fe}^{3+}$ -oxides and  $\text{Fe}^{3+}$ -sulfates occur in the overlying sediments. This is indicated most clearly by the narrow peak that develops at  $\sim 0.75$   $\mu\text{m}$ , between the 0.53 and 0.86  $\mu\text{m}$  absorptions, particularly in the Rockytop and Devils Tanyard members (Figure 3). Furthermore, most of the rocks of the sediments exposed at the fan front show both stronger hydration features than the igneous rocks of the Máaz and Séítah formations, as well as comparable or stronger  $\text{Fe}^{3+}$ -oxides signatures (Figure 5). The correlation of stronger  $\text{Fe}^{3+}$ -related features with stronger  $\text{H}_2\text{O}$  features in both the igneous and sedimentary rocks suggests that the aqueous alteration might have occurred under oxidizing conditions, as opposed to dissolution under reducing conditions and subsequent anhydrous oxidation. This correlation also implies that the sedimentary fan front rocks experienced greater interaction with oxidizing fluids or were more susceptible to alteration compared with the igneous floor rocks.

In addition to these clear changes in Fe-mineralogy expressed in electronic absorptions and  $\text{H}_2\text{O}$  in the 1.9  $\mu\text{m}$  vibrational absorption, there are subtle changes in the metal-OH feature near 2.3  $\mu\text{m}$ . This feature occurs at shorter wavelengths ( $\sim 2.29$   $\mu\text{m}$ ) for  $\text{Fe}^{3+}$ -phyllosilicates such as nontronite and hisingerite and longer wavelengths ( $\sim 2.35$   $\mu\text{m}$ ) for trioctahedral smectites with dominantly  $\text{Fe}^{2+}$  (e.g., ferrosaponite) or for phases like serpentine (e.g., Fox et al., 2021). Carbonates also absorb near 2.3  $\mu\text{m}$ . In the Máaz formation, rock spectra typically exhibit a weak 2.3  $\mu\text{m}$  absorption band centered at a shorter wavelength ( $< 2.29$   $\mu\text{m}$ ), indicative of minor  $\text{Fe}^{3+}$ -phyllosilicates (Mandon et al., 2023). In the Séítah formation, the 2.3  $\mu\text{m}$  band was typically a doublet, with very weak  $\sim 2.29$   $\mu\text{m}$  band ( $\text{Fe}^{3+}$ -OH) and associated with a longer wavelength 2.32  $\mu\text{m}$  absorption (Mg-OH or  $\text{CO}_3$ ), indicating that  $\text{Fe}^{3+}$ -bearing phyllosilicates were present as well as an Mg-OH bearing phase and/or carbonates (Mandon et al., 2023). Except for Amalik, where the 2.3  $\mu\text{m}$  band is centered at 2.33  $\mu\text{m}$  and interpreted to be due to Mg-OH in serpentine, fan sedimentary rocks are associated with a 2.3  $\mu\text{m}$  absorption band centered at 2.30–2.31  $\mu\text{m}$  (Dehouck et al., 2023; Figures 3 and 4). This indicates that the phyllosilicates associated with fan sedimentary rocks have less  $\text{Fe}^{3+}$  in their octahedral sites compared to the igneous floor. This might imply that, compared to the crater floor, at the fan front the protolith composition or the properties of the altering fluid(s) promoted more Fe precipitating into oxides compared to phyllosilicates, or that some Fe-phyllosilicates subsequently altered to Fe-oxides. Alternatively, the phyllosilicates of the fan could be detrital—there are Fe/Mg-

phyllosilicates in the watershed of Jezero's western fan with a similar absorption position (e.g., Mustard et al., 2008).

### 5.1.2. Variability of Fe Oxidation Within the Western Fan

Most of the members of the fan front show dominant Fe<sup>3+</sup>-related absorptions except for the Amalik member, which is dominated by the signature of Fe<sup>2+</sup> carriers (olivine, but possibly ferrous phyllosilicates as well). The main bearers of Fe<sup>3+</sup> are Fe<sup>3+</sup>-oxides, including crystalline red hematite and are found directly underneath Amalik in the lowermost portions of the fan at Kaguyak, as well as above it in the Devils Tanyard and Rockytop members. At Devils Tanyard, possible additional Fe<sup>3+</sup> carriers include phyllosilicates (Dehouck et al., 2023) and at Hogwallow Flats, Fe<sup>3+</sup> is also possibly present in minor phyllosilicates (Dehouck et al., 2023) and in the sulfates.

Strikingly, in contrast to the fan front, the sedimentary rocks exposed at the top of the fan do not exhibit the same trends of increasing Fe<sup>3+</sup>-related signatures with enhanced hydration. Despite being also more hydrated than the igneous floor and despite having comparable Fe content compared to the ones exposed at the fan front (~20–25 wt.% FeO<sub>T</sub>; Dehouck et al., 2023), fan top sedimentary rocks show little to no evidence of Fe oxidation, as evidenced by reduced to absent 0.53 and 0.86 μm absorptions (Figures 3 and 4) and an inferred broad Fe<sup>2+</sup> absorption centered between 1.0 and 1.3 μm, consistent with olivine and/or Fe<sup>2+</sup>/Mg-carbonate.

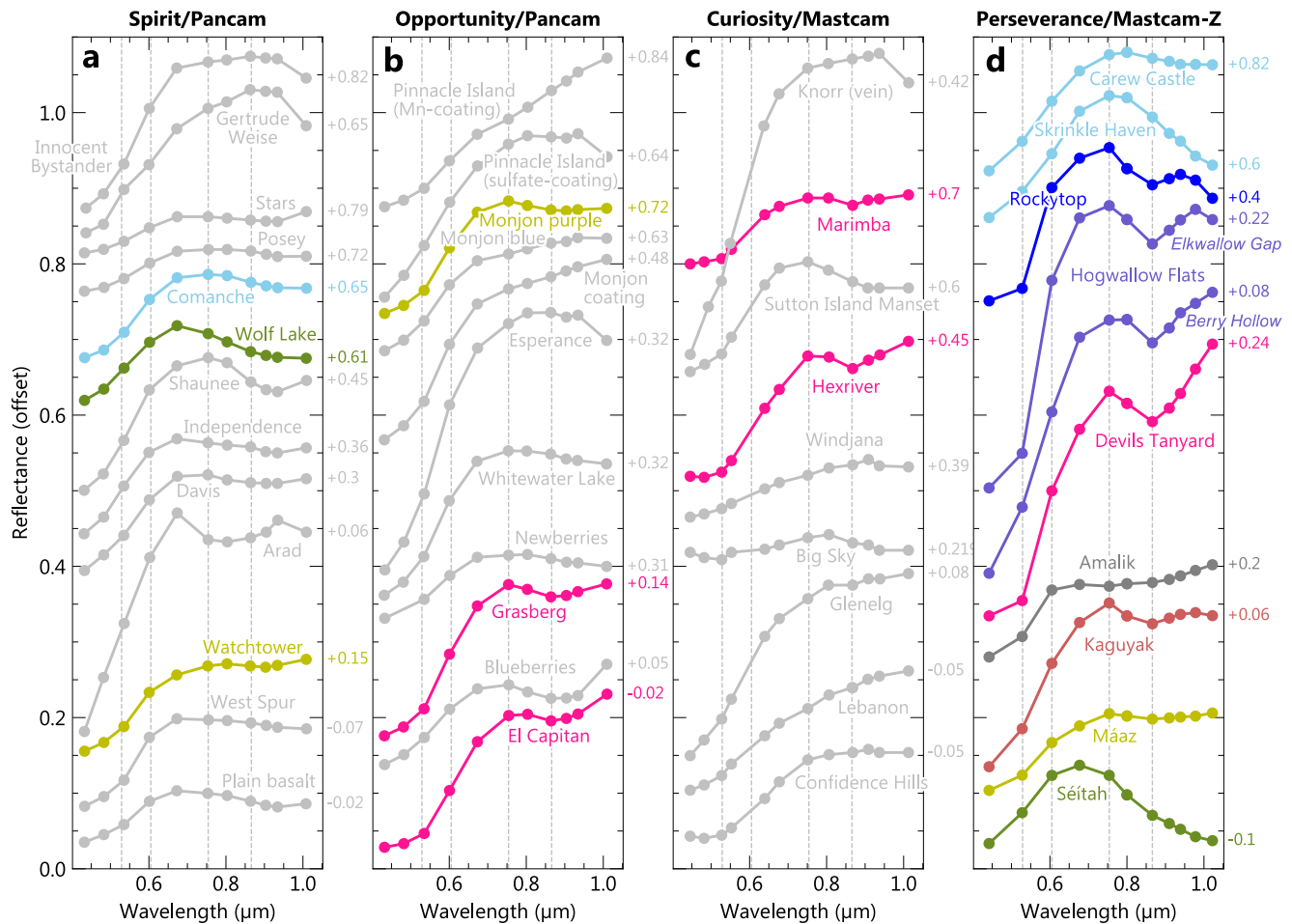
## 5.2. Comparison to Other Landing Sites

Igneous rocks encountered by *Perseverance* share some spectral similarity with basalts in Gusev crater. In particular, Máaz basalts exhibit similar spectral shapes compared to the *Watchtower* class identified by Farrand et al. (2008), with comparable slope in the visible range, reflectance peak near 0.75 μm and comparable 0.53 and 0.86 μm band depths (light yellow green, Figure 9). The *Watchtower* target corresponds to a heavily altered basaltic impact ejecta showing enrichment in Fe-oxides (mainly nano-phase Fe-oxides, hematite and goethite; Fe<sup>3+</sup>/Fe<sub>Total</sub> = 0.83) compared to other basalts in the Columbia Hills (Squyres et al., 2006). Such mineralogy is broadly consistent with our conclusions from Máaz's similar spectra of inferred ferrihydrite and Fe<sup>3+</sup>-phyllosilicate. The Jezero Máaz spectra show a weaker 0.95 μm absorption than similar spectra of the Gale crater *Sutton Island Manset* class (Figure 9c), where Fe<sup>3+</sup>-bearing smectite has been found (Bristow et al., 2018). The weak band near 0.95 μm, typical of these Fe<sup>3+</sup>-smectite species and in contrast to the pronounced feature in the Gale rocks, is consistent with the overall low contribution of phyllosilicates in the Máaz formation, as shown by Wiens et al. (2022) and Mandon et al. (2023).

Séítah rocks are fairly unique between landing sites but are most similar to olivine-rich basalts of the *Seminole/Algonquin* class encountered on the Columbia Hills (Morris et al., 2008; dark olive green in Figure 9). The *Seminole/Algonquin* class target *Wolf Lake* (Figure 9a) and Séítah rocks share similar 0.67–1 μm downturn due to olivine. In *Seminole/Algonquin*-type rocks, olivine accounts for ~70% of the Fe mineralogy (Morris et al., 2008), while Séítah returns ~40 wt.% olivine in bulk rocks (Beyssac et al., 2023; Wiens et al., 2022), with local enrichment up to ~70 wt.% (Liu et al., 2022). The near-infrared downturn is stronger in the spectra of Séítah rocks (Figure 9), as its large phenocrysts tend to deepen absorption strengths (e.g., Carli et al., 2015). This particularly strong signature of olivine of Séítah rocks in the VISIR is similar to orbital observations of the widespread olivine-bearing deposits in the region of Jezero crater (e.g., Hoefen et al., 2003; Mandon et al., 2020; Mustard et al., 2005).

Potential volcanoclastic olivine-rich rocks at the Gusev's Comanche outcrops showed enrichment in Fe<sup>2+</sup>/Mg-carbonates (Morris et al., 2010). Compared to most pristine olivine rocks at Gusev such as target *Wolf Lake*, the *Comanche* target has a similar negative slope in the 0.75–1 μm range, but a reflectance peak shifted to a longer wavelength of >0.75 μm (sky-blue in Figure 9a), likely owing to the presence of Fe<sup>2+</sup> in carbonates, which typically offsets the reflectance peak to a longer wavelength when added to most pure olivine. This is similar to the fan top units, which show similar negative slopes in the 0.75–1 μm range compared to Séítah rocks but have a reflectance peak shifted to longer wavelength, >0.75 μm (sky-blue in Figure 9d), likely owing to more carbonates (also see Section 4.2.6).

The inferred Fe<sup>3+</sup>-oxide (hematite)-bearing rocks at Jezero crater in the Devils Tanyard member have deeper 0.86 μm absorptions compared to the published main spectral classes at the prior landing sites (magenta in Figure 9). The Devils Tanyard spectrum has a 0.86 μm absorption of ~8% relative to the continuum, while the hematite-rich bedrock and blueberries at Meridiani Planum have ~4% (targets *El Capitan* and *Grasberg* in



**Figure 9.** Comparison of Mastcam-Z spectra of the main geological units at Jezero crater discussed here with main Pancam and Mastcam spectral endmembers measured at Meridiani Planum, Gusev Crater and Gale crater. (a) *Spirit*/Pancam spectral endmembers reported by Farrand et al. (2008, 2016). (b) *Opportunity*/Pancam spectral endmembers reported by Farrand et al. (2014, 2016). (c) *Curiosity*/Mastcam spectral endmembers reported by Rice et al. (2022) and *Knorr* vein spectrum shown by Vaniman et al. (2014). (d) *Perseverance*/Mastcam-Z representative spectra of abraded targets of the main bedrock units discussed here, with the exception of the Kaguyak member spectrum (target *Cape Gull*, sol 424), which has been acquired on a non-abraded surface. From bottom to top: *Garde* (sol 209), *Guillaumes* (sol 168), *Cape Gull* (sol 424), *Novarupta* (sol 572), *Rose River Falls* (sol 455), *Berry Hollow* (sol 507), *Elkwallow Gap* (sol 473), *Thornton Gap* (sol 498), *Solva* (sol 751), *Ouzel Falls* (sol 791). All panels share the same Y-axis scale; offsets noted next to each spectrum. Standard deviations of each spectrum not shown for clarity. The color scheme used here draws attention to classes that are qualitatively spectrally similar to the main bedrock units at Jezero crater, as discussed in the main text. Light gray spectra correspond to classes which show little spectral similarity with bedrock encountered at Jezero crater. Dashed lines correspond to Mastcam-Z bandpass centers of interest at 529, 605, 754, and 866 nm.

Figure 9b) and the *Hexriver* spectral class at Gale crater  $\sim 7\%$ . Such absorption strength variability could be explained by more abundant red hematite at Jezero, differences in the grain size and crystallinity of hematite (which strongly affect associated spectral features; e.g., Bishop, 2020), dust cover, or the association of different Fe-phase(s) absorbing at similar wavelengths. The *Hexriver* class at Gale crater as well as *Devils Tanyard* spectrum are more consistent with fine-grained crystalline red hematite, while at Meridiani the red hematite was associated with nano-phase hematite (e.g., target *El Capitan*) or coarse-grained dark red/gray hematite (e.g., Christensen, Bandfield, Clark, et al., 2000; Farrand et al., 2016), which both tend to broaden and decrease the 0.86  $\mu\text{m}$  absorption (e.g., Bishop, 2020). Jarosite was found in association with hematite in Burns formation bedrock (Morris et al., 2006b). As this mineral absorbs in the  $\sim 0.75\text{--}1.4 \mu\text{m}$  range, it should deepen the 0.86  $\mu\text{m}$  band, but associated spectra of *El Capitan* and *Grasberg* show weaker 0.86  $\mu\text{m}$  band depth than the *Hexriver* class and *Devils Tanyard* spectrum. This likely indicates that the contribution of hematite to the 0.86  $\mu\text{m}$  is less important at Meridiani, in agreement with less fine-grained crystalline red hematite.

We note that coarse-grained gray hematite was also detected by ChemCam in gray diagenetic features of Gale's Vera Rubin ridge (Fraeman, Johnson, et al., 2020; L'Haridon et al., 2020), and Horgan, Johnson, et al. (2020) proposed that the spectral variability observed in Mastcam spectra of the ridge bedrock is caused by variability in hematite grain size and crystallinity. The latter has been interpreted by Horgan, Johnson, et al. (2020) as a result of spatially variable dissolution and reprecipitation of red hematite during late diagenesis. No spectra consistent with gray hematite have been clearly identified within Jezero fan sedimentary rocks so far although its spectrally neutral nature reduces its detectability in VISIR.

Several spectral classes are unique to Jezero crater. None of the Pancam spectral classes reported by Farrand et al. (2008, 2013, 2014, 2016) compare with the Amalik spectra with their 0.6  $\mu\text{m}$  "step" feature (dark gray; Figure 9d). Comparison with Mastcam data at Gale crater is more difficult, as the camera lacks a narrowband filter near 0.6  $\mu\text{m}$ , but no evident match is found with any of the spectral classes reported by Rice et al. (2022). The MSL Mastcam spectra either exhibit a reflectance peak past 0.7  $\mu\text{m}$ , a broadly continuous red slope, or a broadly flat spectral shape in the visible (Figure 9c). In Curiosity, the passive mode of ChemCam produces spectra covering a similar spectral range as the UV and VIS spectrometers of SuperCam. Most similar ChemCam endmember spectrum (from data shown by Johnson et al., 2015; Fraeman, Johnson, et al., 2020; Manelski et al., 2023) to the Amalik endmember is found for "gray" class of rocks (e.g., target *Oban* in Fraeman, Johnson, et al., 2020) of the Vera Rubin ridge that contained coarse-grained gray hematite. We note that PIXL and the LIBS instruments did not detect compositions consistent with hematite in gray rock strata at Amalik, which should be expected if abundant and coarse-grained. While the origin of this "step" feature in the Amalik rocks is not understood, it might reflect a unique mineralogic assemblage not reported before on Mars in situ, possibly related to a form of serpentine species (reported by Dehouck et al., 2023) or other minor sulfide or oxide phase(s) (see Section 4.2.2).

Similarly, none of the spectral classes identified from rover exploration prior to Jezero crater match the spectrum of the Hogwallow Flats member on target *Berry Hollow* shown in Figure 9d: a deep 0.86  $\mu\text{m}$  absorption without any significantly strong 0.53  $\mu\text{m}$  absorption. We interpreted the presence of the former and the weakness of the latter, and the presence of a 0.43  $\mu\text{m}$  band (Section 4.2.4), as diagnostic of  $\text{Fe}^{3+}$ -sulfates such as copiapites. While  $\text{Fe}^{3+}$ -sulfates were detected in light-toned soils at Gusev crater (represented by target *Arad* in Figure 9a), the associated Pancam spectrum is significantly different in shape of the 0.8  $\mu\text{m}$  band, which is broader in the spectrum of the *Arad* disturbed soil and centered at shorter wavelength ( $\sim 0.80$   $\mu\text{m}$ ; Figure 9a) compared to Hogwallow Flats bedrock (0.86  $\mu\text{m}$ ; Figure 9a). This is likely due to differences in the  $\text{Fe}^{3+}$ -sulfates content and/or grain size. Hurowitz et al. (2023) proposed that at Hogwallow Flats most of sulfates are  $\text{Fe}^{2+}$ /Mg-bearing, with only a small  $\text{Fe}^{3+}$ -bearing fraction. However,  $\text{Fe}^{3+}$ -sulfates made up to 35 wt.% of the *Arad* soil (Ming et al., 2008; Morris et al., 2008), possibly as a heterogeneous mixture of  $\text{Fe}^{3+}$ -sulfates, including candidates such as ferricopiapite, jarosite, fibroferrite, rhomboclase, and coquimbite (Johnson et al., 2007). While copiapites and jarosite might be present at Hogwallow Flats (Hurowitz et al., 2023; Section 4.2.4),  $\text{Fe}^{3+}$ -sulfates with a 0.8  $\mu\text{m}$  absorption centered at wavelength shorter than 0.86  $\mu\text{m}$  such as fibroferrite and rhomboclase (e.g., Cloutis et al., 2006) have not readily been detected at Hogwallow Flats, hence possibly explaining the difference in band center compared to the  $\text{Fe}^{3+}$ -sulfates soils observed at Gusev crater.

Finally, previously reported spectral classes from Pancam and Mastcam that show strong 0.53 and 0.86  $\mu\text{m}$  absorptions do not exhibit additional 0.75–1  $\mu\text{m}$  negative slope as in the spectra measured at Jezero's Rockytop, which have both features (Figure 9d), and that we interpret as a mixture of olivine and/or Fe-carbonates with fine-grained crystalline red hematite (see Section 4.2.5).

Out of the main Pancam and Mastcam spectral classes reported by Farrand et al. (2008, 2013, 2014, 2016) and Rice et al. (2022), many have yet no spectral equivalent in bedrock members of Jezero. In particular, no Mastcam-Z spectra have a strong 0.55–0.85  $\mu\text{m}$  slope, a reflectance peak near 0.86  $\mu\text{m}$  and a 0.93–1  $\mu\text{m}$  downturn (interpreted as hydration and/or hydroxylation; Rice et al., 2010). These features are observed in the spectra of hydrated Fe-poor rocks observed at other landing sites: silica-rich deposits at Home Plate (targets *Innocent Bystander* and *Gertrude Weise* in Figure 9a) and Ca-sulfates material at Gale crater (target *Knorr* in Figure 9c). While Ca-sulfate veins are reported in Jezero's western fan (mostly in the Hogwallow Flats/Yori Pass members; Nachon et al., 2023), their occurrences are scarce compared to Gale crater where they are abundant (e.g., Kronyak et al., 2019; Nachon et al., 2014; Rapin et al., 2016).

At Gale crater, bedrock enriched in dark Mn-oxides has been observed (corresponding to spectral class/target *Windjana* in Figure 9c). While coatings enriched in Mn-oxides have been detected in the Hogwallow Flats

member (Lanza et al., 2023), no elemental data show significant enrichment in Mn (Gasda et al., 2022) nor do Mastcam-Z spectra show compelling evidence of Mn-oxides within fan sedimentary bedrock (Figure 9). This indicates that the highly oxidizing conditions required to precipitate Mn-oxides at Gale crater were not favored during deposition or diagenesis of Jezero's sedimentary rocks, or that any Mn-oxide was dissolved by reducing water after deposition.

### 5.3. Origin of the Color Banding

In both the Amalik and Rockytop members, a likely similar process produced recurring intervals of red and gray layers, correlated with hydration and Fe<sup>3+</sup>-oxide variability. Color variations related to Fe<sup>3+</sup>-oxides variations have already been reported in situ on Mars at Gale crater (e.g., Haber et al., 2022; Horgan, Johnson, et al., 2020). However, what is novel about the color banding at Jezero is that it is observed at a fine cm-scale along layers traceable horizontally over several meters (Figure 7).

At Gale crater, Horgan, Johnson, et al. (2020) described color variation within the sedimentary rocks of the Vera Rubin ridge, where red bedrock was associated with the presence of fine-grained and poorly crystalline hematite and gray rocks with coarser-grained hematite. The gray portions were interpreted as resulting from the “bleaching” of the red rocks, by dissolution of red hematite and reprecipitation into clusters of larger grains of gray hematite, a process that can happen on Earth during diagenesis and fluid circulation in sedimentary rocks (e.g., Eichhubl et al., 2004). The main driver for variability of bleaching along the Vera Rubin ridge was hypothesized to be local differences in grain size of the initial material, leading to variable permeability and porosity. By contrast, at Jezero crater, PIXL and LIBS instruments did not detect composition consistent with hematite in gray-hued rock strata at Amalik and Rockytop, which should be detected if abundant and coarse-grained. It is possible (amongst other hypotheses) that small amounts of gray hematite are responsible for darkening of these rocks, but is less favored, as both the 0.53 and 0.86 μm would be reduced. Here, only the 0.53 μm band seems affected, pointing to a variability in other Fe<sup>3+</sup>-oxides. Hence, we can probably exclude the hypothesis of a hematite bleaching process similar to that postulated for Gale crater. However, it is possible that initial differences in porosity and grain size of the bedrock led to differences in Fe<sup>3+</sup>-oxides precipitation along a diagenetic flow path. At Rockytop, the gray bands are raised compared to the red ones (Figure 7f), likely indicating differences in erodibility and hence porosity/grain size.

On Earth, alternating bands of Fe<sup>3+</sup>-oxides in rocks are formed through a variety of processes. One of the most typical examples is Banded Iron Formations (BIFs): these chemical sedimentary rocks mostly found in the Precambrian record show sub-mm to m-scale banding of alternating Fe-rich (hematite, magnetite) and Fe-poor (usually Si-rich) layers (e.g., Klein, 2005), where the banding has been attributed to varying oxidation conditions in Fe<sup>2+</sup>-rich waters in contact with an early reduced atmosphere during sediment deposition. The mechanism(s) of Fe oxidation is still debated, but most plausible scenarios include localized photosynthetic or photoferrotrophic activity as well as UV-photo-oxidation, both mechanisms that could have been controlled by astronomic or seasonal cycles (for a review, see Posth et al., 2013). The rocks at Amalik and Rockytop do not fall into the category of BIFs mineralogically because most of their Fe is in mafic minerals or their alteration products.

Alternatively, the banding could have a diagenetic origin. Some repeating Fe-oxide patterns in rocks are lumped into the term “Liesegang bands.” These bands typically develop during diagenesis in porous rocks such as sandstones through precipitation of Fe along the path of a diffusing fluid. For example, in “zebra rocks,” Kawahara et al. (2022) proposed that rhythmic Fe-oxide bands were induced by acidic groundwater fluids enriched in Fe<sup>2+</sup> percolating through carbonate-bearing sedimentary rocks. In this example, Fe-oxides precipitate at the reaction front as dissolution of carbonates buffers the fluid to higher pH. When the reaction is exhausted, Fe-oxide precipitation stops and the reaction front moves forward starting to form a new Fe-oxide band a few cm away from the previous one. Carbonate dissolution promotes porosity and hence fluid diffusion and banding formation. A similar mechanism of Fe-oxide precipitation via pH-buffering by carbonates was proposed for the hematite spherules observed by the *Opportunity* rover at Meridiani Planum (Yoshida et al., 2018). Wang et al. (2015) showed that a spatially repetitive pattern can autonomously emerge from the pore-space-confined Ostwald ripening (where smaller particles diffuse to larger ones to increase thermodynamic stability) of Fe<sup>3+</sup>-oxides precipitated along a flow path. The pattern type can be used as an indicator of paleo-flows. Spherules (such as the ones found at Meridiani Planum on Mars) are preferentially formed under stagnant hydrologic conditions, whereas bands form during persistent water circulation. In these models, the bands exhibit spacing from the mm to sub-mm scale, which is comparable to the banding observed at Amalik and Rockytop. However, they are not

necessarily parallel to the stratification, while at Amalik and Rockytop, the color banding appears tied to the stratification of the bedrock.

Finally, other scenarios could be invoked to explain the banding observed at Amalik and Rockytop, such as a change in sediment source, episodic lake dry-outs, or late surface oxidation after the end of the lake activity. But these scenarios are unlikely given the lack of textural heterogeneity at Amalik, overall lack of unconformities, and regularity over small scales of these layers. Episodic changes in atmospheric composition can also be considered but would typically occur on longer time/vertical scales than the deposition of just the few meters of sandstones observed at Rockytop. Hence, we retain the three following hypotheses as the most plausible: (a) varying balance between water level and groundwater infiltration during deposition, (b) varying intensity of the effect of photo-oxidation and (c) infiltration of fluids in bedrock of varying porosity during diagenesis.

In the scenario involving varying balances of surface and groundwater, formation of some  $\text{Fe}^{3+}$ -oxides could occur during deposition, primarily by episodic sedimentation of insoluble  $\text{Fe}^{3+}$  from oxidation of soluble  $\text{Fe}^{2+}$  in Fe-bearing waters. The banding would record varying water levels and groundwater infiltration (the source of reduced Fe-bearing fluids) during deposition. There would be a chemocline with surface waters oxidized due to contact with an oxidizing atmosphere or UV-driven oxidation (e.g., Hurowitz et al., 2017) depth. Given the recurrence of the alternating intervals, these processes could be linked to seasonal cycles with the amount of groundwater input and lake levels controlled by the balance between evaporation and precipitation, the temperature (controlling convective mixing of the lake water), and/or wind speed and direction.

Under the scenario of varying intensity of the effect of photo-oxidation, the water column in which the sediments of Amalik and Rockytop would have been sufficiently oxidized from UV flux to allow precipitation of  $\text{Fe}^{3+}$ -oxides (e.g., Loche et al., 2022). Variability of solar flux on the lake water surface could have been driven by seasons or by episodic freezing of the lake surface, where low insolation periods would have been associated with less precipitation of  $\text{Fe}^{3+}$ -oxides, forming the darker bands.

Tebolt et al. (2023) proposed that the Amalik member is part of a Bouma sequence and was deposited in a turbiditic flow. Such a hypothesis would be inconsistent with alternating deposition of Fe-oxides modulated by variation of the lake level and groundwater inputs or with varying intensity of the effect of photo-oxidation, because in a turbidite scenario, the whole Amalik member would have been deposited during a single rapid gravity flow event. If validated, the turbidite hypothesis would favor a banding driven by infiltration of fluids in bedrock of varying porosity during diagenesis.

## 5.4. Implications for Environmental History

### 5.4.1. Hydration as a Driver for Bedrock Oxidation

From the observations discussed previously, we can draw hypotheses regarding the alteration history of the rocks at Jezero. First, the signatures of Fe oxidation are correlated with those of hydration (Section 5.1). This likely reflects aqueous alteration by oxidizing fluids, forming  $\text{Fe}^{3+}$ -oxides at the expense of primary ferrous minerals. The correlation between hydration and  $\text{Fe}^{3+}$  disfavors the hypothesis of dry surface oxidation after the end of the lake activity being the major oxidation event(s) of the bedrock.

The fan sedimentary rocks show more extensive signs of past interaction with water compared to the igneous floor rocks, possibly because of their higher porosity, of higher alteration kinetics, or because of alteration events of greater spatial/temporal water availability (e.g., the igneous floor units could have been isolated from the lake by deposition of more impermeable layers). The most common Fe-oxide of the igneous floor is inferred to be ferrihydrite, a poorly crystalline nanomineral Fe-oxide species, as opposed to the crystalline red hematite present at the overlying fan sedimentary rocks. This is also consistent with the fan front having experienced longer-lived water-rock interactions, higher alteration kinetics and/or higher degrees of diagenesis compared to the igneous crater floor.

### 5.4.2. Significance of Fe Oxidation in the Sediments Exposed at the Fan Front

The spectral data presented here show that the Amalik member could be associated with  $\text{Fe}^{2+}$ -clay minerals, and other  $\text{Fe}^{2+}$ -bearing secondary minerals were detected in the fan ( $\text{Fe}^{2+}$ /Mg-carbonates at Rockytop, and  $\text{Fe}^{2+}$ /Mg-sulfates at Hogwallow Flats; Dehouck et al., 2023; Hurowitz et al., 2023). The occurrence of secondary ferrous

species in these sedimentary rocks, whether transported or authigenic, implies water-rock interactions under poorly oxidizing conditions during deposition of the strata exposed at the fan front or that the oxidation reactions did not fully progress due to short-lived water-rock interaction or low temperatures. Yet, despite the presence of these ferrous secondary phases, some of the sedimentary rocks exposed at the fan front (e.g., Devils Tanyard) show strong signatures of  $\text{Fe}^{3+}$ . Hence, the co-occurrence of ferric and ferrous phases implies conditions favoring oxidation at some point in Jezero's history, but the timing and origin of the oxidation are inadequately constrained by the observations.

In a scenario where Fe-redox variations are lake-driven (i.e., Hurowitz et al., 2017), materials would have been deposited in a redox-stratified lake in contact with an oxidized surface (resulting from a broadly oxidized atmosphere and/or caused by surface UV radiation). Varying water level and groundwater infiltration, and hence varying chemocline level, would have been responsible for variable  $\text{Fe}^{3+}$ -oxide precipitation—similarly but on a broader scale than what can be proposed for the cm-scale banding observed at Amalik and Rockytop (see Section 5.3).

While a lake in contact with an oxidized surface during sediment deposition is possible, it cannot be excluded that most or portions of the lake were reduced during emplacement of the main units, and that oxidation happened later during post-depositional circulation of oxidizing fluids or during episodic drying and exposure of specific intervals to oxidative weathering. While no sedimentary structures such as scours are observed in the stratigraphy to indicate drying up periods, the following diagenetic-related features are observed:

- At Amalik, the more strongly oxidized features are diagenetic in origin, including red hematite-rich veins (*Bruin Bay* target, Figure 6), while most of the dark-toned bedrock appears reduced. The hypothesis of Tebolt et al. (2023) that Amalik and Kaguyak being deposited during a single gravity flow event could be consistent with a diagenetic origin for  $\text{Fe}^{3+}$ -oxide formation. In that scenario, the underlying and now more oxidized Kaguyak member exhibits a coarser grain size (Stack et al., 2024) and hence a higher porosity, and was therefore more prone to fluid circulation and hence oxidation by fluids.
- In the Devils Tanyard and Hogwallow Flats members, veins/mineralized ridges, concretions and deformed strata are commonly observed (Nachon et al., 2023; Broz et al., 2024; Kalucha et al., 2023; Stack et al., 2024; Figure 6). These are the members at the fan front area showing the strongest oxidation features in the spectra described here. In these two members, the red hematite and  $\text{Fe}^{3+}$ -sulfate signatures are not readily concentrated along fractures, concretions, or in deformed strata (Figures 3 and 6), which indicates either that the oxidation of the materials is pre-diagenetic or that it was pervasive enough to fully oxidize the strata. We note that these two members are where Lanza et al. (2023) detected Mn-oxides, which require potent oxidizing conditions to form. However, because they are present as varnishes or coatings, they are very likely decorrelated from the main aqueous activity of the site and might have formed more recently than the other oxides detected here.

Both syndepositional and diagenetic processes could have been at play to form the oxidized materials in the Jezero crater fan. At the global scale of Mars, significant Fe-bearing secondary minerals found from orbit and in situ in Hesperian terrains are sulfates that usually form under acidic conditions (e.g., jarosite; Klingelhöfer et al., 2004; Thollot et al., 2012) and  $\text{Fe}^{3+}$ -oxides, such as hematite, likely resulting from episode(s) of diagenesis (e.g., Christensen, Bandfield, Clark, et al., 2000; Clark et al., 2005; Glotch et al., 2006; McLennan et al., 2005), and contrasting with the Noachian clay-rich mineralogy (e.g., Carter et al., 2013; Ehlmann et al., 2011; Poulet et al., 2005). At Gale crater, hematite is reported in the sedimentary rocks comprising the Murray Formation, and has been interpreted as authigenic (Hurowitz et al., 2017) or diagenetic (Rampe et al., 2017)—likely formed during Hesperian time, given the lower bound age provided by the emplacement of the crater at the Noachian/Hesperian boundary (Thomson et al., 2011). Hence, a line of comparison can be drawn with the Jezero system, whose late fluvial/lacustrine activity likely overlapped with Gale's (Mangold et al., 2020). The crystalline hematite and other oxidized hydrated minerals such as the  $\text{Fe}^{3+}$ -sulfates we report in the strata exposed at the fan front might have formed under similar processes that seemed to mostly affect Hesperian terrains (Bibring et al., 2007). This is of particular importance as the associated sedimentary rocks have been sampled for return to Earth (Bosak et al., 2024) as part of the Mars Sample Return program and could be relics of alteration processes characteristic of both the Noachian (possibly the Fe/Mg-clay minerals detected by Dehouck et al., 2023 if detrital) and the overprint of this Hesperian-style alteration forming  $\text{Fe}^{3+}$ -oxides.

Interestingly, the sediments at Jezero crater show overall less extensive signs of diagenesis than those at Gale crater. There is less variation in oxides (e.g., lack of clear gray hematite or Mn-oxide detection in bedrock) and a



lack of Fe/Mn-rich nodules as well as Ca-sulfates or Si-rich veins (see Section 5.2). This is consistent with Jezero fan sedimentary rocks having experienced less intense (perhaps as a result of shallower burial and lower groundwater table) or fewer episodes of diagenesis than the sedimentary rocks of Aeolis Mons.

### 5.4.3. Low Fe Oxidation in the Upper Fan Bedrock

No direct geological contact could be observed between the upper parts of the strata exposed in the fan front area and the Skrinkle Haven and Carew Castle members (fan top area). The latter are stratigraphically higher (Figure 1), and Quantin-Nataf et al. (2023) showed that significant westward erosion affected Jezero's fan; this might imply that the fan front sediment are older layers exposed by erosion. An alternative was proposed by Mangold et al. (2024), who suggested that the architecture of the western fan observed in situ is more consistent with the upper fan having been deposited during higher water level prior to lake level fall progradation of the fan and deposition of the fan front strata.

We show there is a striking difference in Fe oxidation between the front and upper sections of the fan. The low oxidation of Fe in the upper fan units compared to the fan front could be explained by the lower dissolution rate of primary minerals, which can translate into lower cumulative exposure to liquid water and/or possibly at lower temperatures. The sedimentary rocks at the top of the delta were likely deposited in shallow environments (Ives et al., 2023). It is hence most expected that the lower fan rocks were more exposed to liquid water than the rocks exposed in the upper fan, which could have experienced less fluid circulation and perhaps less burial. The latter is in agreement with limited to absent diagenetic features in the upper parts of the fan stratigraphy as well as the preservation of boulder-rich lobes on the top of the delta fan (Kronyak et al., 2023).

Alternatively, episodic evaporation during construction of the fan front area bedrock and exposure to oxidative weathering of these intervals could have led to increased oxidation of Fe compared to the upper fan bedrock. This is supported by the presence of soluble sulfates in Hogwallow Flats strata (Dehouck et al., 2023; Hurowitz et al., 2023), which do not favor prolonged exposure to water after deposition.

The fan top area bedrock shows signatures of Fe<sup>2+</sup>-bearing carbonates (see Section 4.2.6 for Mastcam-Z, Dehouck et al., 2023 for SuperCam, or Phua et al., 2024 for SHERLOC). These carbonates could either be detrital or authigenic—or both. According to the framework proposed by Tosca and McLennan (2006), precipitating Fe<sup>2+</sup>-carbonates from brines without Fe<sup>3+</sup>-oxides means that oxidation was slow enough for Fe<sup>2+</sup> to remain in solution. In this model, the epochs associated with the emplacement of the fan top deposits at Jezero could have been associated with a more reducing atmosphere compared to the fan front emplacement.

Other alternatives exist but are less favored. A change of source rocks could induce less oxidized materials deposited in the upper fan and more oxidized ones at the front. While we cannot fully rule out this hypothesis, we note that no red hematite was reported from orbit in the watershed, although surveys in the visible and near-infrared are still ongoing (e.g., Riu et al., 2023). This likely means that its concentration in the strata of the broader fan front area is likely associated with processes that occurred during or after sediment transport and deposition in Jezero, and is not inherited from earlier processes occurring in the watershed.

### 5.5. Implications for Astrobiology and Sample Return

The western fan sedimentary rocks show stronger hydration signals than the igneous rocks located in the Máaz and Séítah areas, indicating a higher degree of interaction between rock and water in the past. The presence of Fe<sup>3+</sup>-oxides and Fe<sup>3+</sup>-sulfates in the strata exposed at the fan front indicates that Fe oxidation processes have taken place, which could have been favorable for a chemolithotrophic environment, a habitat dominated by microorganisms whose metabolism is based on the oxidation of inorganic substrates to acquire the necessary energy for their development.

Plausible explanations for the color banding observed in specific intervals of the western fan stratigraphy at Jezero include the presence of slight changes in redox conditions in time and space during deposition of sediments. Independent of the origin of the redox variations, this implies the prior existence of zones of redox disequilibria at small scales in the aqueous system of Jezero (i.e., the interaction of more oxidizing fluids with more reduced ones), and possibly within the sediments, which on Earth is associated with enhanced microbial activity (e.g., Bochet et al., 2020).

The darkening agent of the serpentine-bearing rocks at Amalik could include (among other hypotheses) magnetite. In serpentinization settings, this mineral is of interest for habitability. Fe oxidation of serpentine and magnetite releases  $H_2$ , a strong greenhouse gas that might have been implicated in warming early Mars (Ramirez et al., 2014; Wordsworth et al., 2021) and that can be used as an energy source for microbial communities (e.g., Schulte et al., 2006).

To understand Mars' biopotential, it is crucial to not only find habitable environments but also to have good preservation potential for any biosignatures. Some areas of the fan front at Jezero appear to be highly oxidized, possibly resulting from diagenetic fluid activity, which is typically considered detrimental to good organic preservation. In contrast, the uppermost fan strata are very poorly oxidized, which could increase the biosignature preservation potential of associated samples (samples *Melyn* and *Otis Peak*). However, oxidation is not always detrimental to biosignature preservation. Some work on terrestrial analogs indicates that high organic preservation can occur in highly oxidized areas if the oxidation products are well-crystallized, which can contribute to the permineralization of the cells. In the fan front area, the strong oxidation features usually correspond to the presence of crystalline hematite, which could be favorable to microorganism preservation (Allen et al., 2001) compared to the igneous rocks where most of the oxides were poorly crystalline (Mandon et al., 2023). Future analysis of the samples of this work after return to Earth will elucidate the presence of organic matter and biosignatures in these rocks.

## 6. Summary and Conclusion

In this contribution, we combined the reflectance spectra measured by the Mastcam-Z and SuperCam instruments onboard the Mars 2020 *Perseverance* rover to inform the Fe mineralogy in Jezero's crater floor igneous rocks and sedimentary rocks of an ancient delta fan. Our findings can be summarized as follows.

The content and nature of  $Fe^{3+}$  and  $Fe^{2+}$  minerals are variable at Jezero crater. Compared to the igneous floor where small amounts of  $Fe^{3+}$ -phyllosilicates and poorly crystalline  $Fe^{3+}$ -oxyhydroxides (e.g., ferrihydrite) were observed (Horgan et al., 2023; Mandon et al., 2023; Rice et al., 2023), more significant signatures of  $Fe^{3+}$ -oxides (mostly fine-grained crystalline red hematite) and  $Fe^{3+}$ -sulfates (potentially copiapites) occur in the strata exposed at the fan front, which also show stronger signatures of hydration. Notably, oxidation of Fe is not readily observed in the upper part of the fan stratigraphy, which shows similar levels of hydration as the bedrock encountered in the fan front area.

Comparing Mastcam-Z spectra collected at Jezero crater to the main spectral endmembers measured at Gusev crater and Meridiani Planum by the Pancam instruments, and at Gale crater by the Mastcam instrument shows similarities between the landing sites. In particular, the Máaz formation basalts (Jezero crater) exhibit spectra comparable to most heavily oxidized basalts at Gusev. The Jezero fan spectra consistent with hematite show mostly fine-grained crystalline hematite, while coarser-grained crystalline hematite spectra were additionally observed at Meridiani Planum and Gale crater. Of interest are spectral types observed at other landing sites but not yet in the bedrock of Jezero crater (e.g., consistent with materials mostly composed of hydrated Fe-poor species such as hydrated silica), but also spectral types that are possibly reported for the first time in landed exploration at Jezero crater. This includes spectral features associated with the Amalik member, where a "step" feature at  $0.6 \mu m$  is observed. Future work (e.g., from returned sample analysis) is necessary to constrain the nature of the possible phase(s) responsible for its presence.

We interpret the variability in hydration and content and crystallinity of Fe-oxides between the western fan and the igneous floor as evidence for the fan front bedrock to be composed of materials that experienced more vigorous water-rock interactions and/or higher degrees of diagenesis under oxidizing conditions. We propose that the upper part of the delta fan was most likely deposited under an atmosphere in a reduced state or during short-lived aqueous activity of liquid water in contact with an oxidized atmosphere. Although evidence for secondary fluids percolating through parts of the sedimentary rocks is reported at the front of the fan (e.g., Nachon et al., 2023), the timing and origin of oxidation of the most oxidized strata remain unresolved and could have happened either during deposition or during diagenesis. In the latter scenario, episode(s) of diagenesis affecting the western fan of Jezero would have been less abundant or of weaker intensity than what was reported at Gale crater, as evidenced by less variability of Fe-oxides and lack of Fe-poor hydrated veins (e.g., hydrated silica) in the western fan. Samples collected for a return to Earth might record alteration processes inherited from the Noachian watershed as well as the diagenetic alteration typically observed on Hesperian terrains.

We also report on the discovery of alternating cm-scale bands of red and gray layers, traceable over several meters horizontally, and correlated with hydration and Fe<sup>3+</sup>-oxide variability, which has not yet been reported elsewhere in situ on Mars, and which occur on two members of different mineralogical compositions in Jezero's fan front area. The most plausible explanation includes variation of lake levels and groundwater infiltration (syn-depositional variations), possibly as seasonal processes, or diagenetic overprint of oxidized fluids percolating through strata of variable permeability.

Redox gradients were likely present in the aqueous system of Jezero, which is an important requirement for habitability. While significant Fe oxidation of the sedimentary rocks present at the western fan front of Jezero is observed (which could be detrimental to organic matter preservation), we note that Fe-oxides are mostly crystalline in the form of hematite, which could contribute to the permineralization of biological structures. The uppermost strata of the fan are mostly preserved from oxidation, which increases their biosignature preservation potential.

Representative samples of the main geological units described here have been sampled by the rover for return to Earth and further characterization, a major objective being the assessment of the past habitability of the site and the presence of biosignatures. In particular, linking redox states and textural mineralogy (e.g., with XANES micro-mapping as well as electron probe and SEM/EDX) will refine the partitioning of reduced and oxidized Fe in the various minerals, the state of the Noachian/Hesperian atmosphere and test the hypotheses elaborated here.

### Conflict of Interest

The authors declare no conflicts of interest relevant to this study.

### Data Availability Statement

All data are available in the NASA Planetary Data System (Bell & Maki, 2020; Wiens & Maurice, 2021).

### Acknowledgments

The authors are truly grateful for the Mastcam-Z, SuperCam and Mars 2020 hardware operations teams for their investment in the mission. L. M. was supported by a Texaco Postdoctoral prize fellowship awarded by the Division of Geological and Planetary Sciences of Caltech. J. R. J. and J. I. N. were supported by ASU subcontract 15-707 (1511125) and J. R. J. also by JPL subcontract 1532432. R. C. W. is supported by NASA contract NNN15AZ24I as part of NASA's Mars Exploration Program. F. G. was supported by the internal INTA project DAXE S. IGS22001. B. L. E. was supported by a NASA Mastcam-Z Co-investigator award.

### References

- Allen, C. C., Westall, F., & Schelble, R. T. (2001). Importance of a Martian hematite site for astrobiology. *Astrobiology*, *1*, 111–123. <https://doi.org/10.1089/153110701750137495>
- Arvidson, R. E., Squyres, S. W., Morris, R. V., Knoll, A. H., Gellert, R., Clark, B. C., et al. (2016). High concentrations of manganese and sulfur in deposits on Murray Ridge, Endeavour Crater, Mars. *American Mineralogist*, *101*(6), 1389–1405. <https://doi.org/10.2138/am-2016-5599>
- Bell, J. F., & Maki, J. N. (2020). Mars 2020 mast camera zoom bundle, from Arizona State University Mastcam-Z Instrument Team, calibrated products. <https://doi.org/10.17189/q3ts-c749>
- Bell, J. F., Maki, J. N., Mehall, G. L., Ravine, M. A., Caplinger, M. A., Bailey, Z. J., et al. (2021). The Mars 2020 perseverance rover mast camera Zoom (Mastcam-Z) multispectral, stereoscopic imaging investigation. *Space Science Reviews*, *217*(1), 24. <https://doi.org/10.1007/s11214-020-00755-x>
- Bell, J. F. I., Godber, A., McNair, S., Caplinger, M. A., Maki, J. N., Lemmon, M. T., et al. (2017). The Mars Science Laboratory Curiosity rover Mastcam instruments: Preflight and in-flight calibration, validation, and data archiving. *Earth and Space Science*, *4*(7), 396–452. <https://doi.org/10.1002/2016EA000219>
- Bell, J. F. I., Squyres, S. W., Herkenhoff, K. E., Maki, J. N., Arneson, H. M., Brown, D., et al. (2003). Mars exploration rover Athena Panoramic camera (Pancam) investigation. *Journal of Geophysical Research*, *108*(E12). <https://doi.org/10.1029/2003JE002070>
- Beysac, O., Forni, O., Cousin, A., Udry, A., Kah, L. C., Mandon, L., et al. (2023). Petrological traverse of the olivine cumulate Séítah formation at Jezero crater, Mars: A perspective from SuperCam onboard perseverance. *Journal of Geophysical Research: Planets*, *128*(7), e2022JE007638. <https://doi.org/10.1029/2022JE007638>
- Bibring, J.-P., Arvidson, R. E., Gendrin, A., Gondet, B., Langevin, Y., Le Mouélic, S., et al. (2007). Coupled ferric oxides and sulfates on the Martian surface. *Science*, *317*(5842), 1206–1210. <https://doi.org/10.1126/science.1144174>
- Bibring, J.-P., Langevin, Y., Gendrin, A., Gondet, B., Poulet, F., Berthé, M., et al. (2005). Mars surface diversity as revealed by the OMEGA/Mars express observations. *Science*, *307*(5715), 1576–1581. <https://doi.org/10.1126/science.1108806>
- Biemann, K., Oro, J., Toulmin, P., III., Orgel, L. E., Nier, A. O., Anderson, D. M., et al. (1977). The search for organic substances and inorganic volatile compounds in the surface of Mars. *Journal of Geophysical Research*, *82*(28), 4641–4658. <https://doi.org/10.1029/JS082i028p04641>
- Bishop, J. L. (2020). Visible and near-infrared reflectance spectroscopy laboratory spectra of geologic materials. In J. L. Bishop, J. F. Bell, III., & J. E. Moersch (Eds.), *Remote compositional analysis-techniques for understanding spectroscopy, mineralogy, and geochemistry of planetary surfaces*.
- Bishop, J. L., Dobrea, E. Z. N., McKeown, N. K., Parente, M., Ehlmann, B. L., Michalski, J. R., et al. (2008). Phyllosilicate diversity and past aqueous activity revealed at Mawrth Vallis, Mars. *Science*, *321*(5890), 830–833. <https://doi.org/10.1126/science.1159699>
- Bishop, J. L., & Murad, E. (2002). Spectroscopic and geochemical analyses of ferrihydrite from springs in Iceland and applications to Mars. *Geological Society, London, Special Publications*, *202*(1), 357–370. <https://doi.org/10.1144/GSL.SP.2002.202.01.18>
- Bochet, O., Bethencourt, L., Dufresne, A., Farasin, J., Pédro, M., Labasque, T., et al. (2020). Iron-oxidizer hotspots formed by intermittent oxic-anoxic fluid mixing in fractured rocks. *Nature Geoscience*, *13*(2), 149–155. <https://doi.org/10.1038/s41561-019-0509-1>
- Bosak, T., Shuster, D. L., Weiss, B., Mayhew, L. E., Scheller, E. L., Siljestroem, S., et al. (2024). Astrobiological potential of rocks acquired by the perseverance rover at the front of the western sediment fan in Jezero crater, Mars. In *55th Lunar and Planetary Science Conference*.

- Boynton, W. V., Taylor, G. J., Evans, L. G., Reedy, R. C., Starr, R., Janes, D. M., et al. (2007). Concentration of H, Si, Cl, K, Fe, and Th in the low- and mid-latitude regions of Mars. *Journal of Geophysical Research*, *112*(E12). <https://doi.org/10.1029/2007JE002887>
- Bristow, T. F., Bish, D. L., Vaniman, D. T., Morris, R. V., Blake, D. F., Grotzinger, J. P., et al. (2015). The origin and implications of clay minerals from Yellowknife Bay, Gale crater, Mars. *American Mineralogist*, *100*(4), 824–836. <https://doi.org/10.2138/am-2015-5077CCBYNCND>
- Bristow, T. F., Rampe, E. B., Achilles, C. N., Blake, D. F., Chipera, S. J., Craig, P., et al. (2018). Clay mineral diversity and abundance in sedimentary rocks of Gale crater, Mars. *Science Advances*, *4*(6), eaar3330. <https://doi.org/10.1126/sciadv.aar3330>
- Broz, A. P., Horgan, B., Kalucha, H., Johnson, J. R., Royer, C., Dehouck, E., et al. (2024). Biosignature preservation potential of sulfate-rich rocks from Hogwallow Flats, Jezero Crater, Mars. In *Paper presented at the 55th Lunar and Planetary Science Conference (LPSC)*, Woodlands, TX.
- Carli, C., Serventi, G., & Sgavetti, M. (2015). VNIR spectral characteristics of terrestrial igneous effusive rocks: Mineralogical composition and the influence of texture. *Geological Society, London, Special Publications*, *401*(1), 139–158. <https://doi.org/10.1144/SP401.19>
- Carter, J., Poulet, F., Bibring, J.-P., Mangold, N., & Murchie, S. (2013). Hydrous minerals on Mars as seen by the CRISM and OMEGA imaging spectrometers: Updated global view. *Journal of Geophysical Research: Planets*, *118*(4), 831–858. <https://doi.org/10.1029/2012JE004145>
- Chemtob, S. M., Nickerson, R. D., Morris, R. V., Agresti, D. G., & Catalano, J. G. (2015). Synthesis and structural characterization of ferrous trioctahedral smectites: Implications for clay mineral genesis and detectability on Mars. *Journal of Geophysical Research: Planets*, *120*(6), 1119–1140. <https://doi.org/10.1002/2014JE004763>
- Chemtob, S. M., Nickerson, R. D., Morris, R. V., Agresti, D. G., & Catalano, J. G. (2017). Oxidative alteration of ferrous smectites and implications for the redox evolution of early Mars. *Journal of Geophysical Research: Planets*, *122*(12), 2469–2488. <https://doi.org/10.1002/2017JE005331>
- Chevrier, V., Poulet, F., & Bibring, J.-P. (2007). Early geochemical environment of Mars as determined from thermodynamics of phyllosilicates. *Nature*, *448*(7149), 60–63. <https://doi.org/10.1038/nature05961>
- Christensen, P. R., Bandfield, J. L., Clark, R. N., Edgett, K. S., Hamilton, V. E., Hoefen, T., et al. (2000). Detection of crystalline hematite mineralization on Mars by the thermal Emission spectrometer: Evidence for near-surface water. *Journal of Geophysical Research*, *105*(E4), 9623–9642. <https://doi.org/10.1029/1999JE001093>
- Christensen, P. R., Bandfield, J. L., Smith, M. D., Hamilton, V. E., & Clark, R. N. (2000). Identification of a basaltic component on the Martian surface from thermal emission spectrometer data. *Journal of Geophysical Research*, *105*(E4), 9609–9621. <https://doi.org/10.1029/1999JE001127>
- Clark, B. C., Baird, A. K., Rose, H. J., Toulmin, P., Keil, K., Castro, A. J., et al. (1976). Inorganic analyses of Martian surface samples at the Viking landing sites. *Science*, *194*(4271), 1283–1288. <https://doi.org/10.1126/science.194.4271.1283>
- Clark, B. C., Morris, R. V., McLennan, S. M., Gellert, R., Jolliff, B., Knoll, A. H., et al. (2005). Chemistry and mineralogy of outcrops at Meridiani Planum. *Earth and Planetary Science Letters*. Sedimentary Geology at Meridiani Planum, Mars, *240*(1), 73–94. <https://doi.org/10.1016/j.epsl.2005.09.040>
- Clark, R. N., King, T. V. V., Klejwa, M., Swayze, G. A., & Vergo, N. (1990). High spectral resolution reflectance spectroscopy of minerals. *Journal of Geophysical Research*, *95*(B8), 12653–12680. <https://doi.org/10.1029/JB095iB08p12653>
- Clarke, R. N. (1999). Spectroscopy of rocks and minerals, and principles of spectroscopy, remote sensing for the Earth sciences. *Man. In Remote Sens* (3rd ed., pp. 3–58). John Wiley Sons.
- Clavé, E., Benzerara, K., Meslin, P.-Y., Forni, O., Royer, C., Mandon, L., et al. (2023). Carbonate detection with SuperCam in igneous rocks on the floor of Jezero crater, Mars. *Journal of Geophysical Research: Planets*, *128*(6), e2022JE007463. <https://doi.org/10.1029/2022JE007463>
- Cloutis, E. A., Hawthorne, F. C., Mertzman, S. A., Krenn, K., Craig, M. A., Marcino, D., et al. (2006). Detection and discrimination of sulfate minerals using reflectance spectroscopy. *Icarus*, *184*(1), 121–157. <https://doi.org/10.1016/j.icarus.2006.04.003>
- Dehouck, E., Forni, O., Quantin-Nataf, C., Beck, P., Mangold, N., Royer, C., et al. (2023). Overview of the bedrock geochemistry and mineralogy observed by SuperCam during perseverance's delta front campaign. In *54th Lunar and Planetary Science Conference* (p. 2862). Lunar and Planetary Institute.
- Dehouck, E., Gaudin, A., Chevrier, V., & Mangold, N. (2016). Mineralogical record of the redox conditions on early Mars. *Icarus*, *271*, 67–75. <https://doi.org/10.1016/j.icarus.2016.01.030>
- Dehouck, E., Gaudin, A., Mangold, N., Lajaunie, L., Dauzères, A., Grauby, O., & Le Menn, E. (2014). Weathering of olivine under CO<sub>2</sub> atmosphere: A Martian perspective. *Geochimica et Cosmochimica Acta*, *135*, 170–189. <https://doi.org/10.1016/j.gca.2014.03.032>
- Ehlmann, B. L., Mustard, J. F., Murchie, S. L., Bibring, J.-P., Meunier, A., Fraeman, A. A., & Langevin, Y. (2011). Subsurface water and clay mineral formation during the early history of Mars. *Nature*, *479*(7371), 53–60. <https://doi.org/10.1038/nature10582>
- Ehlmann, B. L., Mustard, J. F., Murchie, S. L., Poulet, F., Bishop, J. L., Brown, A. J., et al. (2008). Orbital identification of carbonate-bearing rocks on Mars. *Science*, *322*(5909), 1828–1832. <https://doi.org/10.1126/science.1164759>
- Ehlmann, B. L., Mustard, J. F., Swayze, G. A., Clark, R. N., Bishop, J. L., Poulet, F., et al. (2009). Identification of hydrated silicate minerals on Mars using MRO-CRISM: Geologic context near Nili Fossae and implications for aqueous alteration. *Journal of Geophysical Research*, *114*(E2). <https://doi.org/10.1029/2009JE003339>
- Eichhubl, P., Taylor, W. L., Pollard, D. D., & Aydin, A. (2004). Paleo-fluid flow and deformation in the Aztec Sandstone at the Valley of Fire, Nevada—Evidence for the coupling of hydrogeologic, diagenetic, and tectonic processes. *Geological Society of America Bulletin*, *116*(9), 1120–1136. <https://doi.org/10.1130/B25446.1>
- Farley, K. A., Stack, K. M., Shuster, D. L., Horgan, B. H. N., Hurowitz, J. A., Tarnas, J. D., et al. (2022). Aqueously altered igneous rocks sampled on the floor of Jezero crater, Mars. *Science*, *377*(6614), eabo2196. <https://doi.org/10.1126/science.abo2196>
- Farley, K. A., Williford, K. H., Stack, K. M., Bhartia, R., Chen, A., de la Torre, M., et al. (2020). Mars 2020 mission overview. *Space Science Reviews*, *216*(8), 142. <https://doi.org/10.1007/s11214-020-00762-y>
- Farrand, W. H., Bell, J. F., Johnson, J. R., Rice, M. S., & Hurowitz, J. A. (2013). VNIR multispectral observations of rocks at Cape York, Endeavour crater, Mars by the Opportunity rover's Pancam. *Icarus*, *225*(1), 709–725. <https://doi.org/10.1016/j.icarus.2013.04.014>
- Farrand, W. H., Bell, J. F., III, Johnson, J. R., Arvidson, R. E., Crumpler, L. S., Hurowitz, J. A., & Schröder, C. (2008). Rock spectral classes observed by the Spirit Rover's Pancam on the Gusev Crater Plains and in the Columbia Hills. *Journal of Geophysical Research*, *113*(E12). <https://doi.org/10.1029/2008JE003237>
- Farrand, W. H., Bell, J. F., III, Johnson, J. R., Rice, M. S., Jolliff, B. L., & Arvidson, R. E. (2014). Observations of rock spectral classes by the Opportunity Rover's Pancam on northern Cape York and on Matijevic Hill, Endeavour Crater, Mars. *Journal of Geophysical Research: Planets*, *119*(11), 2349–2369. <https://doi.org/10.1002/2014JE004641>
- Farrand, W. H., Johnson, J. R., Rice, M. S., Wang, A., & Bell, J. F. (2016). VNIR multispectral observations of aqueous alteration materials by the Pancams on the Spirit and Opportunity Mars exploration rovers. *American Mineralogist*, *101*(9), 2005–2019. <https://doi.org/10.2138/am-2016-5627>

- Fassett, C. I., & Head, J. W. (2005). Fluvial sedimentary deposits on Mars: Ancient deltas in a crater lake in the Nili Fossae region. *Geophysical Research Letters*, 32(14). <https://doi.org/10.1029/2005GL023456>
- Fouchet, T., Reess, J.-M., Montmessin, F., Hassen-Khodja, R., Nguyen-Tuong, N., Humeau, O., et al. (2022). The SuperCam infrared spectrometer for the perseverance rover of the Mars 2020 mission. *Icarus*, 373, 114773. <https://doi.org/10.1016/j.icarus.2021.114773>
- Fox, V. K., Kupper, R. J., Ehlmann, B. L., Catalano, J. G., Razzell-Hollis, J., Abbey, W. J., et al. (2021). Synthesis and characterization of Fe(III)-Fe(II)-Mg-Al smectite solid solutions and implications for planetary science. *American Mineralogist*, 106(6), 964–982. <https://doi.org/10.2138/am-2020-7419CCBYNCND>
- Fraeman, A. A., Edgar, L. A., Rampe, E. B., Thompson, L. M., Frydenvang, J., Fedo, C. M., et al. (2020). Evidence for a diagenetic origin of Vera Rubin ridge, Gale crater, Mars: Summary and synthesis of curiosity's exploration campaign. *Journal of Geophysical Research: Planets*, 125(12), e2020JE006527. <https://doi.org/10.1029/2020JE006527>
- Fraeman, A. A., Johnson, J. R., Arvidson, R. E., Rice, M. S., Wellington, D. F., Morris, R. V., et al. (2020). Synergistic ground and orbital observations of iron oxides on Mt. Sharp and Vera Rubin ridge. *Journal of Geophysical Research: Planets*, 125(9), e2019JE006294. <https://doi.org/10.1029/2019JE006294>
- Garczynski, B. J., Bell, J. F., III, Horgan, B. H. N., Johnson, J. R., Rice, M. S., Vaughan, A., et al. (2022). Perseverance and the purple coating: A Mastcam-Z multispectral story. In *LPI contributions* (p. 2346).
- Gasda, P. J., Lanza, N., Madariaga, J. M., Arana, G., Castro Ortiz de Pinedo, K., Gómez, F., et al. (2022). Searching for redox stratification in the Jezero crater delta 2022. *AGU Fall Meeting 2022* (p. P52C-1559).
- Gendrin, A., Mangold, N., Bibring, J.-P., Langevin, Y., Gondet, B., Poulet, F., et al. (2005). Sulfates in martian layered terrains: The OMEGA/Mars express view. *Science*, 307(5715), 1587–1591. <https://doi.org/10.1126/science.1109087>
- Glavin, D. P., Freissinet, C., Miller, K. E., Eigenbrode, J. L., Brunner, A. E., Buch, A., et al. (2013). Evidence for perchlorates and the origin of chlorinated hydrocarbons detected by SAM at the Rocknest aeolian deposit in Gale Crater. *Journal of Geophysical Research: Planets*, 118(10), 1955–1973. <https://doi.org/10.1002/jgre.20144>
- Glotch, T. D., Bandfield, J. L., Christensen, P. R., Calvin, W. M., McLennan, S. M., Clark, B. C., et al. (2006). Mineralogy of the light-toned outcrop at Meridiani Planum as seen by the Miniature Thermal Emission spectrometer and implications for its formation. *Journal of Geophysical Research*, 111(E12). <https://doi.org/10.1029/2005JE002672>
- Goudge, T. A., Milliken, R. E., Head, J. W., Mustard, J. F., & Fassett, C. I. (2017). Sedimentological evidence for a deltaic origin of the western fan deposit in Jezero crater, Mars and implications for future exploration. *Earth and Planetary Science Letters*, 458, 357–365. <https://doi.org/10.1016/j.epsl.2016.10.056>
- Haber, J. T., Horgan, B., Fraeman, A. A., Johnson, J. R., Bell, J. F., III, Rice, M. S., et al. (2022). Mineralogy of a possible ancient lakeshore in the sutton Island member of Mt. Sharp, Gale crater, Mars, from mastcam multispectral images. *Journal of Geophysical Research: Planets*, 127(10), e2022JE007357. <https://doi.org/10.1029/2022JE007357>
- Hecht, M. H., Kounaves, S. P., Quinn, R. C., West, S. J., Young, S. M. M., Ming, D. W., et al. (2009). Detection of perchlorate and the soluble chemistry of Martian soil at the phoenix lander site. *Science*, 325(5936), 64–67. <https://doi.org/10.1126/science.1172466>
- Hem, J. D., & Cropper, W. H. (1962). Chemistry of iron in natural water. *United States Geological Survey*, 1–31.
- Hoefen, T. M., Clark, R. N., Bandfield, J. L., Smith, M. D., Pearl, J. C., & Christensen, P. R. (2003). Discovery of olivine in the Nili Fossae region of Mars. *Science*, 302(5645), 627–630. <https://doi.org/10.1126/science.1089647>
- Horgan, B., Udry, A., Rice, M., Alwmark, S., Amundsen, H. E. F., Bell, J. F., III, et al. (2023). Mineralogy, morphology, and emplacement history of the Maaz formation on the Jezero crater floor from orbital and rover observations. *Journal of Geophysical Research: Planets*, 128(8), e2022JE007612. <https://doi.org/10.1029/2022JE007612>
- Horgan, B. H. N., Anderson, R. B., Dromart, G., Amador, E. S., & Rice, M. S. (2020). The mineral diversity of Jezero crater: Evidence for possible lacustrine carbonates on Mars. *Icarus*, 339, 113526. <https://doi.org/10.1016/j.icarus.2019.113526>
- Horgan, B. H. N., Johnson, J. R., Fraeman, A. A., Rice, M. S., Seeger, C., Bell, J. F., III, et al. (2020). Diagenesis of Vera Rubin ridge, Gale crater, Mars, from Mastcam multispectral images. *Journal of Geophysical Research: Planets*, 125(11), e2019JE006322. <https://doi.org/10.1029/2019JE006322>
- Hunt, G. R., & Ashley, R. P. (1979). Spectra of altered rocks in the visible and near infrared. *Economic Geology*, 74(7), 1613–1629. <https://doi.org/10.2113/gsecongeo.74.7.1613>
- Hurowitz, J. A., Grotzinger, J. P., Fischer, W. W., McLennan, S. M., Milliken, R. E., Stein, N., et al. (2017). Redox stratification of an ancient lake in Gale crater, Mars. *Science*, 356(6341), eaah6849. <https://doi.org/10.1126/science.aah6849>
- Hurowitz, J. A., Tice, M. M., Allwood, A. C., Cable, M. L., Bosak, T., Broz, A., et al. (2023). The petrogenetic history of the Jezero crater delta front from microscale observations by the Mars 2020 pixl instrument. In *54th Lunar and Planetary Science Conference 2023*. Lunar and Planetary Institute, The Woodlands (Texas).
- Ives, L., Stack, K., Gupta, S., Grotzinger, J. P., Lamb, M. P., Barnes, R., et al. (2023). Reassessing the sedimentary depositional origin of the Jezero crater western Fan's curvilinear Unit: Reconciling orbital and rover observations. *AGU23*.
- Johnson, J. R., Bell, J. F., Bender, S., Blaney, D., Cloutis, E., DeFlores, L., et al. (2015). ChemCam passive reflectance spectroscopy of surface materials at the Curiosity landing site, Mars. *Icarus*, 249, 74–92. Special Issue: First Year of MSL. <https://doi.org/10.1016/j.icarus.2014.02.028>
- Johnson, J. R., Bell, J. F., Bender, S., Blaney, D., Cloutis, E., Ehlmann, B., et al. (2016). Constraints on iron sulfate and iron oxide mineralogy from ChemCam visible/near-infrared reflectance spectroscopy of Mt. Sharp basal units, Gale Crater, Mars. *American Mineralogist*, 101(7), 1501–1514. <https://doi.org/10.2138/am-2016-5553>
- Johnson, J. R., Bell, J. F., III, Cloutis, E., Staid, M., Farrand, W. H., McCoy, T., et al. (2007). Mineralogic constraints on sulfur-rich soils from Pancam spectra at Gusev crater, Mars. *Geophysical Research Letters*, 34(13). <https://doi.org/10.1029/2007GL029894>
- Johnson, J. R., Leget, C., Wiens, R. C., Newell, R. T., Cloutis, E., Forni, O., et al. (2022). Visible wavelength spectroscopy (400–1020 Nm) of surface materials at Jezero crater, Mars, from supercam and Mastcam-Z. Presented at the *53rd Lunar and Planetary Science Conference* (p. 1254).
- Kalucha, H., Broz, A. P., Fischer, W. W., Gasda, P. J., & Randazzo, N. (2023). In-situ alteration in sulfate rich units of Jezero Crater, Mars. In *Paper presented at the 54th Lunar and Planetary Science Conference (LPSC), Woodlands, TX*.
- Kawahara, H., Yoshida, H., Yamamoto, K., Katsuta, N., Nishimoto, S., Umemura, A., & Kuma, R. (2022). Hydrothermal formation of Fe-oxide bands in zebra rocks from northern Western Australia. *Chemical Geology*, 590, 120699. <https://doi.org/10.1016/j.chemgeo.2021.120699>
- Klein, C. (2005). Presidential Address to the mineralogical Society of America, Boston, November 6, 2001: Some Precambrian banded iron-formations (BIFs) from around the world: Their age, geologic setting, mineralogy, metamorphism, geochemistry, and origin. *American Mineralogist*, 90(10), 1473–1499. <https://doi.org/10.2138/am.2005.1871>
- Klingelhöfer, G., Morris, R. V., Bernhardt, B., Schröder, C., Rodionov, D. S., de Souza, P. A., et al. (2004). Jarosite and hematite at Meridiani Planum from Opportunity's Mössbauer spectrometer. *Science*, 306(5702), 1740–1745. <https://doi.org/10.1126/science.1104653>

- Kong, W. G., Wang, A., Freeman, J. J., & Sobron, P. (2011). A comprehensive spectroscopic study of synthetic Fe<sup>2+</sup>, Fe<sup>3+</sup>, Mg<sup>2+</sup> and Al<sup>3+</sup> copiapite by Raman, XRD, LIBS, MIR and vis-NIR. *Journal of Raman Spectroscopy*, 42(5), 1120–1129. <https://doi.org/10.1002/jrs.2790>
- Kronyak, R. E., Kah, L. C., Edgett, K. S., VanBommel, S. J., Thompson, L. M., Wiens, R. C., et al. (2019). Mineral-filled fractures as indicators of multigenerational fluid flow in the Pahrump Hills member of the Murray Formation, Gale crater, Mars. *Earth and Space Science*, 6(2), 238–265. <https://doi.org/10.1029/2018EA000482>
- Kronyak, R. E., Stack-Morgan, K. M., Sholes, S. F., Sun, V. Z., Gupta, S., Shuster, D. L., & Caravaca, G. (2023). Geomorphology and relative ages of channel belt deposits in Jezero's western delta. In *54th Lunar and Planetary Science Conference (LPSC 2023)* (p. 2067). Lunar and Planetary Institute.
- Lane, M. D., Morris, R. V., Mertzman, S. A., & Christensen, P. R. (2002). Evidence for platy hematite grains in Sinus Meridiani, Mars. *Journal of Geophysical Research*, 107(E12), 9-1–9-15. <https://doi.org/10.1029/2001JE001832>
- Lanza, N., Gasda, P., Ollila, A., Chide, B., Garczynski, B., Johnson, J., et al. (2023). A varnish-like high-manganese rock coating in Jezero crater, Mars. *Presented at the EGU23, Copernicus Meetings*. <https://doi.org/10.5194/egusphere-egu23-10757>
- Lanza, N. L., Fischer, W. W., Wiens, R. C., Grotzinger, J., Ollila, A. M., Cousin, A., et al. (2014). High manganese concentrations in rocks at Gale crater, Mars. *Geophysical Research Letters*, 41(16), 5755–5763. <https://doi.org/10.1002/2014GL060329>
- Lapo, K. E., Vaughan, A. F., Rice, M. S., Mandon, L., Johnson, J. R., & Garczynski, B. J. (2024). Distinguishing iron carbonates from olivines in visible to near-infrared. *Presented at the 55th Lunar and Planetary Science Conference*.
- L'Haridon, J., Mangold, N., Fraeman, A. A., Johnson, J. R., Cousin, A., Rapin, W., et al. (2020). Iron mobility during diagenesis at Vera Rubin ridge, Gale crater, Mars. *Journal of Geophysical Research: Planets*, 125(11), e2019JE006299. <https://doi.org/10.1029/2019JE006299>
- Liu, Y., Tice, M. M., Schmidt, M. E., Treiman, A. H., Kizovski, T. V., Hurowitz, J. A., et al. (2022). An olivine cumulate outcrop on the floor of Jezero crater, Mars. *Science*, 377(6614), 1513–1519. <https://doi.org/10.1126/science.abo2756>
- Liu, Y., & Wang, A. (2015). Dehydration of Na-jarosite, ferricopiapite, and rhombochalcite at temperatures of 50 and 95°C: Implications for Martian ferric sulfates. *Journal of Raman Spectroscopy*, 46(5), 493–500. <https://doi.org/10.1002/jrs.4655>
- Loche, M., Fabre, S., Meslin, P.-Y., Cousin, A., Lanza, N., Kah, L. C., et al. (2022). Exploring the formation of the Mn-P-Fe-Mg enrichment of the groken nodules in Gale crater with source-to-sink geochemical modeling. *Presented at 53rd Lunar and Planetary Science Conference (Vol. 2678, p. 1274)*.
- Loeffler, M. J., & Prince, B. S. (2022). A possible explanation for the blue spectral slope observed on B-type asteroids. *Icarus*, 376, 114881. <https://doi.org/10.1016/j.icarus.2022.114881>
- Mandon, L., Quantin-Nataf, C., Royer, C., Beck, P., Fouchet, T., Johnson, J. R., et al. (2023). Reflectance of Jezero crater floor: 2. Mineralogical interpretation. *Journal of Geophysical Research: Planets*, 128(7), e2022JE007450. <https://doi.org/10.1029/2022JE007450>
- Mandon, L., Quantin-Nataf, C., Thollot, P., Mangold, N., Lozac'h, L., Dromart, G., et al. (2020). Refining the age, emplacement and alteration scenarios of the olivine-rich unit in the Nili Fossae region, Mars. *Icarus*, 336, 113436. <https://doi.org/10.1016/j.icarus.2019.113436>
- Manelski, H. T., Sheppard, R. Y., Fraeman, A. A., Wiens, R. C., Johnson, J. R., Rampe, E. B., et al. (2023). Compositional variations in sedimentary deposits in Gale crater as observed by ChemCam passive and active spectra. *Journal of Geophysical Research: Planets*, 128(3), e2022JE007706. <https://doi.org/10.1029/2022JE007706>
- Mangold, N., Caravaca, G., Gupta, S., Williams, R. M. E., Dromart, G., Gasnault, O., et al. (2024). Architecture of fluvial and deltaic deposits exposed along the eastern edge of the western fan of Jezero crater, Mars. *Journal of Geophysical Research: Planets*, 129(3), e2023JE008204. <https://doi.org/10.1029/2023JE008204>
- Mangold, N., Dromart, G., Ansan, V., Salese, F., Kleinhans, M. G., Massé, M., et al. (2020). Fluvial regimes, morphometry, and age of Jezero crater paleolake inlet valleys and their exobiological significance for the 2020 rover mission landing site. *Astrobiology*, 20(8), 994–1013. <https://doi.org/10.1089/ast.2019.2132>
- Mangold, N., Gupta, S., Gasnault, O., Dromart, G., Tarnas, J. D., Sholes, S. F., et al. (2021). Perseverance rover reveals an ancient delta-lake system and flood deposits at Jezero crater, Mars. *Science*, 374(6568), 711–717. <https://doi.org/10.1126/science.abl4051>
- Mansbach, E. N., Kizovski, T. V., Mandon, L., Scheller, E. L., Bosak, T., Wiens, R. C., et al. (2023). Identification of magnetic phases by perseverance and implications for paleomagnetic analysis of returned samples 2806, 2072. *Presented at 54th Lunar and Planetary Science Conference*.
- Maurice, S., Wiens, R. C., Bernardi, P., Caïs, P., Robinson, S., Nelson, T., et al. (2021). The SuperCam instrument suite on the Mars 2020 rover: Science objectives and mast-unit description. *Space Science Reviews*, 217(3), 47. <https://doi.org/10.1007/s11214-021-00807-w>
- McElroy, M. B. (1972). Mars: An evolving atmosphere. *Science*, 175(4020), 443–445. <https://doi.org/10.1126/science.175.4020.443>
- McLennan, S. M., Bell, J. F., Calvin, W. M., Christensen, P. R., Clark, B. C., de Souza, P. A., et al. (2005). Provenance and diagenesis of the evaporite-bearing Burns formation, Meridiani Planum, Mars. *Earth and Planetary Science Letters*, Sedimentary Geology at Meridiani Planum, Mars. 240(1), 95–121. <https://doi.org/10.1016/j.epsl.2005.09.041>
- Merusi, M., Kinch, K. B., Madsen, M. B., Bell, J. F., III, Maki, J. N., Hayes, A. G., et al. (2022). The Mastcam-Z Radiometric calibration targets on NASA's perseverance rover: Derived Irradiance time-Series, dust deposition, and performance over the first 350 sols on Mars. *Earth and Space Science*, 9(12), e2022EA002552. <https://doi.org/10.1029/2022EA002552>
- Michalski, J., Poulet, F., Bibring, J.-P., & Mangold, N. (2010). Analysis of phyllosilicate deposits in the Nili Fossae region of Mars: Comparison of TES and OMEGA data. *Icarus. Solar Wind Interactions with Mars*, 206(1), 269–289. <https://doi.org/10.1016/j.icarus.2009.09.006>
- Miller, S. L. (1953). A production of amino acids under possible primitive Earth conditions. *Science*, 117(3046), 528–529. <https://doi.org/10.1126/science.117.3046.528>
- Milliken, R. E. (2020). RELAB spectral library bundle.
- Ming, D. W., Gellert, R., Morris, R. V., Arvidson, R. E., Brückner, J., Clark, B. C., et al. (2008). Geochemical properties of rocks and soils in Gusev Crater, Mars: Results of the alpha particle X-ray spectrometer from Cumberland ridge to Home Plate. *Journal of Geophysical Research*, 113(E12). <https://doi.org/10.1029/2008JE003195>
- Morris, R. V., Golden, D. C., Bell, J. F., III, Shelfer, T. D., Scheinost, A. C., Hinman, N. W., et al. (2000). Mineralogy, composition, and alteration of Mars Pathfinder rocks and soils: Evidence from multispectral, elemental, and magnetic data on terrestrial analogue, SNC meteorite, and Pathfinder samples. *Journal of Geophysical Research*, 105(E1), 1757–1817. <https://doi.org/10.1029/1999JE001059>
- Morris, R. V., Klingelhöfer, G., Schröder, C., Fleischer, I., Ming, D. W., Yen, A. S., et al. (2008). Iron mineralogy and aqueous alteration from Husband Hill through Home Plate at Gusev Crater, Mars: Results from the Mössbauer instrument on the Spirit Mars exploration rover. *Journal of Geophysical Research*, 113(E12). <https://doi.org/10.1029/2008JE003201>
- Morris, R. V., Klingelhöfer, G., Schröder, C., Rodionov, D. S., Yen, A., Ming, D. W., et al. (2006a). Mössbauer mineralogy of rock, soil, and dust at Gusev crater, Mars: Spirit's journey through weakly altered olivine basalt on the plains and pervasively altered basalt in the Columbia Hills. *Journal of Geophysical Research*, 111(E2). <https://doi.org/10.1029/2005JE002584>

- Morris, R. V., Klingelhöfer, G., Schröder, C., Rodionov, D. S., Yen, A., Ming, D. W., et al. (2006b). Mössbauer mineralogy of rock, soil, and dust at Meridiani Planum, Mars: Opportunity's journey across sulfate-rich outcrop, basaltic sand and dust, and hematite lag deposits. *Journal of Geophysical Research*, *111*(E12). <https://doi.org/10.1029/2006JE002791>
- Morris, R. V., Ruff, S. W., Gellert, R., Ming, D. W., Arvidson, R. E., Clark, B. C., et al. (2010). Identification of carbonate-rich outcrops on Mars by the Spirit Rover. *Science*, *329*(5990), 421–424. <https://doi.org/10.1126/science.1189667>
- Mustard, J. F., Murchie, S. L., Pelkey, S. M., Ehlmann, B. L., Milliken, R. E., Grant, J. A., et al. (2008). Hydrated silicate minerals on Mars observed by the Mars Reconnaissance orbiter CRISM instrument. *Nature*, *454*(7202), 305–309. <https://doi.org/10.1038/nature07097>
- Mustard, J. F., Poulet, F., Gendrin, A., Bibring, J.-P., Langevin, Y., Gondet, B., et al. (2005). Olivine and pyroxene diversity in the crust of Mars. *Science*, *307*(5715), 1594–1597. <https://doi.org/10.1126/science.1109098>
- Nachon, M., Clegg, S. M., Mangold, N., Schröder, S., Kah, L. C., Dromart, G., et al. (2014). Calcium sulfate veins characterized by ChemCam/Curiosity at Gale crater, Mars. *Journal of Geophysical Research: Planets*, *119*(9), 1991–2016. <https://doi.org/10.1002/2013JE004588>
- Nachon, M., López-Reyes, G., Meslin, P.-Y., M. Ollila, A., Mandon, L., Clavé, E., et al. (2023). Light-toned veins and material in Jezero crater, Mars, as seen in-situ via NASA's perseverance rover (Mars 2020 mission): Stratigraphic distribution and compositional results from the supercam instrument. *54th Lunar and Planetary Science Conference 2023* (p. 2673). Lunar and Planetary Institute.
- Navarro-González, R., Vargas, E., de la Rosa, J., Raga, A. C., & McKay, C. P. (2010). Reanalysis of the Viking results suggests perchlorate and organics at midlatitudes on Mars. *Journal of Geophysical Research*, *115*(E12). <https://doi.org/10.1029/2010JE003599>
- Núñez, J. I., Johnson, J. R., Rice, M. S., Horgan, B. N., Vaughan, A., Garczynski, B. J., et al. (2023). Spectral diversity along the delta front in Jezero crater, Mars as seen with Mastcam-Z on the Mars 2020 perseverance rover 2806, 3036. *Presented at 54th Lunar and Planetary Science Conference*.
- Paige, D. A., Hamran, S.-E., Amundsen, H. E. F., Berger, T., Russell, P., Kakaria, R., et al. (2024). Ground penetrating radar observations of the contact between the western delta and the crater floor of Jezero crater, Mars. *Science Advances*, *10*(4), eadi8339. <https://doi.org/10.1126/sciadv.adi8339>
- Phua, Y. Y., Ehlmann, B., Siljeström, S., Czaja, A., Bhartia, R., Minitti, M., et al. (2024). Characterizing hydration carrier phases in altered rocks of Jezero crater fan and floor geologic units with SHERLOC on Mars 2020. *Journal of Geophysical Research: Planets*, *129*(7), e2023JE008251. <https://doi.org/10.1029/2023JE008251>
- Posth, N. R., Konhauser, K. O., & Kappler, A. (2013). Microbiological processes in banded iron formation deposition. *Sedimentology*, *60*(7), 1733–1754. <https://doi.org/10.1111/sed.12051>
- Poulet, F., Bibring, J.-P., Mustard, J. F., Gendrin, A., Mangold, N., Langevin, Y., et al. (2005). Phyllosilicates on Mars and implications for early Martian climate. *Nature*, *438*(7068), 623–627. <https://doi.org/10.1038/nature04274>
- Quantin-Nataf, C., Alwmark, S., Calef, F. J., Lasue, J., Kinch, K., Stack, K. M., et al. (2023). The complex exhumation history of Jezero crater floor unit and its implication for Mars sample return. *Journal of Geophysical Research: Planets*, *128*(6), e2022JE007628. <https://doi.org/10.1029/2022JE007628>
- Ramirez, R. M., Koppurapu, R., Zuger, M. E., Robinson, T. D., Freedman, R., & Kasting, J. F. (2014). Warming early Mars with CO<sub>2</sub> and H<sub>2</sub>. *Nature Geoscience*, *7*(1), 59–63. <https://doi.org/10.1038/ngeo2000>
- Rampe, E. B., Blake, D. F., Bristow, T. F., Ming, D. W., Vaniman, D. T., Morris, R. V., et al. (2020). Mineralogy and geochemistry of sedimentary rocks and eolian sediments in Gale crater, Mars: A review after six Earth years of exploration with Curiosity. *Geochemistry*, *80*(2), 125605. <https://doi.org/10.1016/j.chemer.2020.125605>
- Rampe, E. B., Bristow, T. F., Morris, R. V., Morrison, S. M., Achilles, C. N., Ming, D. W., et al. (2020). Mineralogy of Vera Rubin ridge from the Mars science laboratory CheMin instrument. *Journal of Geophysical Research: Planets*, *125*(9), e2019JE006306. <https://doi.org/10.1029/2019JE006306>
- Rampe, E. B., Ming, D. W., Blake, D. F., Bristow, T. F., Chipera, S. J., Grotzinger, J. P., et al. (2017). Mineralogy of an ancient lacustrine mudstone succession from the Murray formation, Gale crater, Mars. *Earth and Planetary Science Letters*, *471*, 172–185. <https://doi.org/10.1016/j.epsl.2017.04.021>
- Rapin, W., Meslin, P.-Y., Maurice, S., Vaniman, D., Nachon, M., Mangold, N., et al. (2016). Hydration state of calcium sulfates in Gale crater, Mars: Identification of bassanite veins. *Earth and Planetary Science Letters*, *452*, 197–205. <https://doi.org/10.1016/j.epsl.2016.07.045>
- Rice, M. S., Bell, J. F., Cloutis, E. A., Wang, A., Ruff, S. W., Craig, M. A., et al. (2010). Silica-rich deposits and hydrated minerals at Gusev Crater, Mars: Vis-NIR spectral characterization and regional mapping. *Icarus*, *205*(2), 375–395. <https://doi.org/10.1016/j.icarus.2009.03.035>
- Rice, M. S., Johnson, J. R., Million, C. C., St. Clair, M., Horgan, B. N., Vaughan, A., et al. (2023). Spectral variability of rocks and soils on the Jezero crater floor: A summary of multispectral observations from Perseverance's Mastcam-Z instrument. *Journal of Geophysical Research: Planets*, *128*(10), e2022JE007548. <https://doi.org/10.1029/2022JE007548>
- Rice, M. S., Seeger, C., Bell, J., Calef, F., St. Clair, M., Eng, A., et al. (2022). Spectral diversity of rocks and soils in Mastcam observations along the Curiosity Rover's Traverse in Gale crater, Mars. *Journal of Geophysical Research: Planets*, *127*(8), e2021JE007134. <https://doi.org/10.1029/2021JE007134>
- Riu, L., Ody, A., & Carter, J. (2023). Global mapping of hematite at Mars using visible OMEGA/MEx hyperspectral data 2806. *Presented at 54th Lunar and Planetary Science Conference* (p. 1417).
- Royer, C., Fouchet, T., Mandon, L., Montmessin, F., Poulet, F., Forni, O., et al. (2023). Reflectance of Jezero crater floor: 1. Data processing and calibration of the infrared spectrometer (IRS) on SuperCam. *Journal of Geophysical Research: Planets*, *128*, e2022JE007481. <https://doi.org/10.1029/2022JE007481>
- Russell, M. J., & Hall, A. J. (1997). The emergence of life from iron monosulphide bubbles at a submarine hydrothermal redox and pH front. *Journal of the Geological Society*, *154*(3), 377–402. <https://doi.org/10.1144/gsjgs.154.3.0377>
- Scheller, E. L., Hollis, J. R., Cardarelli, E. L., Steele, A., Beegle, L. W., Bhartia, R., et al. (2022). Aqueous alteration processes in Jezero crater, Mars—Implications for organic geochemistry. *Science*, *378*, eabo5204. <https://doi.org/10.1126/science.abo5204>
- Schulte, M., Blake, D., Hoehler, T., & McCollom, T. (2006). Serpentinization and its implications for life on the early Earth and Mars. *Astrobiology*, *6*(2), 364–376. <https://doi.org/10.1089/ast.2006.6.364>
- Simon, J. I., Hickman-Lewis, K., Cohen, B. A., Mayhew, L. E., Shuster, D. L., Debaille, V., et al. (2023). Samples collected from the floor of Jezero crater with the Mars 2020 perseverance rover. *Journal of Geophysical Research: Planets*, *128*(6), e2022JE007474. <https://doi.org/10.1029/2022JE007474>
- Smith, R. J., McLennan, S. M., Achilles, C. N., Dehouck, E., Horgan, B. H. N., Mangold, N., et al. (2021). X-ray amorphous components in sedimentary rocks of Gale crater, Mars: Evidence for ancient formation and Long-lived aqueous activity. *Journal of Geophysical Research: Planets*, *126*(3), e2020JE006782. <https://doi.org/10.1029/2020JE006782>
- Suyres, S. W., Arvidson, R. E., Blaney, D. L., Clark, B. C., Crumpler, L., Farrand, W. H., et al. (2006). Rocks of the Columbia Hills. *Journal of Geophysical Research*, *111*(E2). <https://doi.org/10.1029/2005JE002562>

- Stack, K. M., Ives, L. R. W., Gupta, S., Lamb, M. P., Tebolt, M., Caravaca, G., et al. (2024). Sedimentology and stratigraphy of the Shenandoah formation, western fan, Jezero crater, Mars. *Journal of Geophysical Research: Planets*, *129*(2), e2023JE008187. <https://doi.org/10.1029/2023JE008187>
- Stack, K. M., Williams, N. R., Calef, F., Sun, V. Z., Williford, K. H., Farley, K. A., et al. (2020). Photogeologic map of the perseverance rover field site in Jezero crater constructed by the Mars 2020 science team. *Space Science Reviews*, *216*(8), 127. <https://doi.org/10.1007/s11214-020-00739-x>
- Sun, V. Z., Hand, K. P., Stack, K. M., Farley, K. A., Simon, J. I., Newman, C., et al. (2023). Overview and results from the Mars 2020 perseverance rover's first science campaign on the Jezero crater floor. *Journal of Geophysical Research: Planets*, *128*(6), e2022JE007613. <https://doi.org/10.1029/2022JE007613>
- Tebolt, M., Stack-Morgan, K. M., Goudge, T. A., Gupta, S., Barnes, R., Caravaca, G. & Brown, A. (2023). Characterizing the facies and stratigraphy of the enchanted lake outcrop in Jezero Crater, Mars. In *Paper presented at the 54th Lunar and Planetary Science Conference (LPSC), Woodlands, TX*.
- Thollot, P., Mangold, N., Ansan, V., Le Mouélic, S., Milliken, R. E., Bishop, J. L., et al. (2012). Most Mars minerals in a nutshell: Various alteration phases formed in a single environment in Noctis Labyrinthus. *Journal of Geophysical Research*, *117*(E11). <https://doi.org/10.1029/2011JE004028>
- Thomson, B. J., Bridges, N. T., Milliken, R., Baldrige, A., Hook, S. J., Crowley, J. K., et al. (2011). Constraints on the origin and evolution of the layered mound in Gale crater, Mars using Mars Reconnaissance orbiter data. *Icarus*, *214*(2), 413–432. <https://doi.org/10.1016/j.icarus.2011.05.002>
- Tosca, N. J., & McLennan, S. M. (2006). Chemical divides and evaporite assemblages on Mars. *Earth and Planetary Science Letters*, *241*(1–2), 21–31. <https://doi.org/10.1016/j.epsl.2005.10.021>
- Treiman, A. H., Bish, D. L., Vaniman, D. T., Chipera, S. J., Blake, D. F., Ming, D. W., et al. (2016). Mineralogy, provenance, and diagenesis of a potassic basaltic sandstone on Mars: CheMin X-ray diffraction of the Windjana sample (Kimberley area, Gale crater). *Journal of Geophysical Research: Planets*, *121*(1), 75–106. <https://doi.org/10.1002/2015JE004932>
- Turenne, N., Parkinson, A., Applin, D. M., Mann, P., Cloutis, E. A., & Mertzman, S. A. (2022). Spectral reflectance properties of minerals exposed to martian surface conditions: Implications for spectroscopy-based mineral detection on Mars. *Planetary and Space Science*, *210*, 105377. <https://doi.org/10.1016/j.pss.2021.105377>
- Udry, A., Ostwald, A., Sautter, V., Cousin, A., Beyssac, O., Forni, O., et al. (2023). A Mars 2020 perseverance SuperCam perspective on the igneous nature of the Máaz formation at Jezero Crater and link with Séítah, Mars. *Journal of Geophysical Research: Planets*, *128*(7), e2022JE007440. <https://doi.org/10.1029/2022JE007440>
- Vaniman, D. T., Bish, D. L., Ming, D. W., Bristow, T. F., Morris, R. V., Blake, D. F., et al. (2014). Mineralogy of a Mudstone at Yellowknife Bay, Gale crater, Mars. *Science*, *343*(6169), 1243480. <https://doi.org/10.1126/science.1243480>
- Wadhwa, M. (2001). Redox state of Mars' upper mantle and crust from Eu Anomalies in Shergottite pyroxenes. *Science*, *291*(5508), 1527–1530. <https://doi.org/10.1126/science.1057594>
- Wang, A., & Ling, Z. C. (2011). Ferric sulfates on Mars: A combined mission data analysis of salty soils at Gusev crater and laboratory experimental investigations. *Journal of Geophysical Research*, *116*, E00F17. <https://doi.org/10.1029/2010JE003665>
- Wang, Y., Chan, M. A., & Merino, E. (2015). Self-organized iron-oxide cementation geometry as an indicator of paleo-flows. *Scientific Reports*, *5*(1), 10792. <https://doi.org/10.1038/srep10792>
- Wiens, R. C., & Maurice, S. (2021). Mars 2020 SuperCam bundle. <https://doi.org/10.17189/1522646>
- Wiens, R. C., Maurice, S., Robinson, S. H., Nelson, A. E., Cais, P., Bernardi, P., et al. (2020). The SuperCam instrument suite on the NASA Mars 2020 rover: Body unit and combined system tests. *Space Science Reviews*, *217*(1), 4. <https://doi.org/10.1007/s11214-020-00777-5>
- Wiens, R. C., Udry, A., Beyssac, O., Quantin-Nataf, C., Mangold, N., Cousin, A., et al. (2022). Compositionally and density stratified igneous terrain in Jezero crater, Mars. *Science Advances*, *8*(34), eabo3399. <https://doi.org/10.1126/sciadv.abo3399>
- Wordsworth, R., Kalugina, Y., Lokshtanov, S., Vighasin, A., Ehlmann, B., Head, J., et al. (2017). Transient reducing greenhouse warming on early Mars. *Geophysical Research Letters*, *44*(2), 665–671. <https://doi.org/10.1002/2016GL071766>
- Wordsworth, R., Knoll, A. H., Hurowitz, J., Baum, M., Ehlmann, B. L., Head, J. W., & Steakley, K. (2021). A coupled model of episodic warming, oxidation and geochemical transitions on early Mars. *Nature Geoscience*, *14*(3), 127–132. <https://doi.org/10.1038/s41561-021-00701-8>
- Yoshida, H., Hasegawa, H., Katsuta, N., Maruyama, I., Sirono, S., Minami, M., et al. (2018). Fe-oxide concretions formed by interacting carbonate and acidic waters on Earth and Mars. *Science Advances*, *4*(12), eaau0872. <https://doi.org/10.1126/sciadv.aau0872>
- Zorn, T., Studier, G., Szwarc, T., Jens, E., Tirona, I., & Edelberg, K. (2023). The evolution of surface preparation tools for in situ science on Mars. In *2023 IEEE Aerospace Conference* (pp. 1–19). IEEE.